Computer Simulation Of Lattice Defects In Ni_3Al.

by

PR. Chidambaram

thesis submitted to the Faculty of the

Virginia Polytechnic Institute and State University

in partial fulfillment of the requirements for the degree of

Master of Science

in

Materials Engineering

APPROVED:

Diana Farkas, chairperson

J. L. Lytton

R. E. Swanson

November 1987

Blacksburg, Virginia

Computer Simulation Of Lattice Defects In Ni_3Al.

by

PR. Chidambaram

Diana Farkas, chairperson

Materials Engineering

(ABSTRACT)

Empirically estimated potentials were used to study the defects in Ni_3Al. A computer program which uses the conjugate gradient technique to obtain the relaxed structures was used. Atoms in the vicinity of the planar defects on the (111) plane were found to relax in two different oscillation modes namely the acoustic and optical modes. While the former is similar to the relaxation observed in pure Aluminum or Nickel, the latter was found to be a result of micromoments within the unit cell. The presence of atoms that differ in size and charge are believed to create micro-moments within each unit cell. The energy of a surface seem to depend directly on the atomic density of the terminating plane.

A vacancy prefers to be formed near the boundary rather than in the bulk. The formation of an Nickel vacancy is preferred, also a Nickel vacancy has more activation energy to migrate to the boundary. The effect of the $\Sigma = 5$ boundary seems to be felt only until a distance of approximately 5 Å away from the boundary.

Acknowledgements

The present study is actually a group effort, the author would like to thank all those were involved directly or indirectly in making this work a success.

Innumerable informal discussions that the author had with his advisor, Dr. D. Farkas were of immense help in understanding the problem and comprehending the results. Thanks are due to Dr. E. J. Savino without whose help this study on the defect structures would not be accomplished.Acknowledgements are due to the committee members Dr. J. L. Lytton and Dr. R. E. Swanson for their suggestions.

The potentials used in this study were developed at the Las Alamos National Laboratories, thanks are due to Dr. A. F. Vorter and his colleagues for having provided the data for this project.

The seminar series presented by Dr. S. Rao was of great help in understanding the material presented in chapter 2. The author would like to thank Karen Macleod, Dr. Michael Lewus, who have given many suggestion to improve the presentation of this thesis and Mukundan Rangaswamy for having helped the author solve many computer related problems. Also the author appreciates the help extended by Hemansu Bhatt and Dinesh Bhetadapur.

Table of Contents

List of Illustrations

List of Tables

1.0 Introduction.

There is an increasing interest in characterizing the superalloys, since they seem to have a very good potential for use as high temperature materials. Ni_3Al, one of the commercially available superalloy has the unique property of showing increasing yield strength with increasing test temperature up to approximately 1400 °C [1]. However, it loses its toughness at high temperatures, and often undergoes catastrophic failure at temperatures greater than 1400 ° C. Akoi and Isumi [2] found that this tendency to become embrittled can be overcome by micro-additions of Boron or Hafnium. This alloy, therefore, found unhindered commercial applications. There has been a tremendous amount of research on this material to identify the cause of the benevolent effect of micro-additions of boron. The catastrophic failure is intergranular in nature and occurs along the grain or subgrain boundaries. A fundamental study of the defect interfaces in this material is, therefore, essential for the understanding of the solute interaction with such interfaces.

The ability of a screw dislocation to cross slip plays affects the creep strength of the material. Any kind of a planar defect on the glide planes would act as barriers to the dislocation motion. Consequently a study of the formation energies of various defects on the glide plane could prove useful. The formation of anti phase boundaries by cross slip of forest dislocations is a known cause of work hardening in super alloys [3]. Behavior of atoms close to the defect depends on many different factors, and it is difficult to develop a simple model to describe this behavior. The

primary aim of the present study is to understand the behavior of the atoms around some common defects in Ni_3Al.

Calculations of distortions in the lattice around the defects from first principles has been of particular interest. There are many different techniques that have been developed to describe the behavior of atoms around some simple lattice defects. The static Greens function technique could be used to obtain solutions for the natural vibrations in crystal lattice and for calculating the displacements of atoms close to a point defect. A brief study of this technique was conducted with intention of extending this calculation to stronger defects such as stacking faults, twins, grain boundaries etc. Though an analytical estimation of the displacement field caused by a strong defect is not of much interest, an explanation of the observed oscillations of the atoms could be analytically developed.

Prompted by the failure of analytical techniques to accurately evaluate the displacements around defects, the numerical methods were applied. The computer program that incorporates the Devil code developed by Norgett et al [4]. was used to generate the three dimensional lattice. A defect was then introduced into the lattice and the entire system was relaxed for the lowest energy configuration. The numerical relaxation was carried out using the conjugate gradient technique. In this method, the atoms were moved in $3N$ [1] directions in the process of achieving a relaxed configuration. Though the numerical relaxation technique is capable of handling strong defects, it is highly sensitive to the potential used for the calculation. Potentials are basically the energy terms that describe the interaction of two or more atoms. The potentials that are practically used are empirically calculated and are fitted to the properties of interest. Over the years there has been a growing faith in the empirically estimated potentials; much of this is attributed to exhaustive physical considerations that are taken into account while correcting the potentials. However there could be misgivings about the validity of the absolute value of defect energy as predicted by the numerical techniques but the relative behavior, such as the displacement field obtained from this model has been widely accepted.

---

[1] N is the total number of atoms

The displacement of the atoms parallel and perpendicular to a defect were studied. The magnitude of displacements of the atoms were studied as a function of the distance of the atomic position from the defect. An oscillatory mode of relaxation of atoms from the strained configuration at the defect interface of Ni_3Al was observed.

A detailed study of the interaction of the vacancy with the grain boundary was conducted. The $\Sigma = 5$ [210] (100) boundary in the Ni_3Al was chosen for the calculation. The formation energy of a vacancy was studied as a function of the relative position of the vacancy with respect to the boundary. This type of study is expected to provide a basis for understanding the impurity transport close to the boundary, and therefore give a good idea of the source and sink of the vacancies.

2.0 Theory

Both analytical techniques and numerical relaxation methods have been successfully employed in the past for defect studies. In this chapter a brief description of the analytical technique available for simple defect calculations and a development to explain the oscillatory relaxation modes is discussed. Finally the numerical procedure used to relax the atoms is explained.

2.1 Analytical considerations

Calculations based on first principles are of great importance in predicting the exact behavior of the properties under consideration. Not surprisingly, the research in lattice dynamics dates back to Lifshits (1943-1944). Following the developments in computers the interest in this field expanded very quickly during the 1960's, and has been researched widely in the last two decades. Review articles on this topic have been presented in the conference on defect dynamics at Argonne, U.S.A. [5].

The analytical description of forces on atoms in a crystals involves complex matrix mathematics, and even though the crystal symmetry can be used advantageously, exact solutions

for displacements are difficult to obtain. However, over the years researchers have simplified the treatment with some simplifying assumptions. Most analytical calculations are based on the Taylor series expansion of the potential energy term. The mathematics becomes difficult to handle when this expansion is carried out to many terms. The simplest model uses only terms up to order two. This approximation is called the **Harmonic Approximation** and is explained below.

2.1.1 Harmonic Approximation for perfect Lattice

Consider an infinite lattice [2] composed of many unit cells with each cell bound by three orthogonal vectors $\vec{a}_1, \vec{a}_2, \vec{a}_3$. Let $\vec{X}(l)$ be the position vector that describes the atom at the l'th unit cell. In terms of the orthogonal vectors this can be described as,

$$X_i = l\, a_i \tag{2.1}$$

In case of primitive cells this relation could be used to describe all the atoms. However, in a superlattice as in the Ni_3Al where there are more than one atom in a unit cell, we need another constant to describe the exact atomic position. Therefore we need to introduce a new parameter, k.

$$X_i = l\, a_i + k\, a_i = (l + k)\, a_i \tag{2.2}$$

This could be represented as X (lk), such that k describes the different atoms in the same unit cell.

To describe the potential energy of a crystal we can use the **adiabatic approximation.** By this approximation the electrons are always assumed to be in ground state with respect to the nucleus. This assumption allows one to eliminate the degrees of freedom arising from the movement of the electrons. The potential energy of the crystal is now a function of the atom position

---

[2] an infinite lattice assumption is necessary if surface effects are to be eliminated

alone. When this potential energy is expanded as a Taylor series expansion in powers of the atomic displacements u (lk), we have

$$\Phi = \Phi_o + \sum_{lk} \Phi_{,i}\ u_i(l,k) + \frac{1}{2} \sum_{\substack{lk \\ l'k'}} \Phi_{,ij}\ (lk;l'k')\ u_i(lk)\ u_j(l'k') + \ldots\ldots \qquad (2.3)$$

In the above the expansion the unharmonic terms are neglected, consequently this expansion is called the **Harmonic approximation of the potential energy** . The notations used here are the Einstein's tensorial notations, which are explained elsewhere [6]. A brief description of the terms in eq.(2.7) is given below.

$$\Phi_{,i}(lk) = \frac{\partial \Phi}{\partial u_i(lk)} \qquad (2.4)$$

evaluated at the equilibrium position. It is apparent that $\Phi_{,i}$ (lk) is the negative of the force acting on the atom at the equilibrium position.

$$\Phi_{,ij}(lk\,;l'k') = \frac{\partial^2 \Phi}{\partial u_i(lk)\ \partial u_j(l'k')} \qquad (2.5)$$

The coefficients on the left of the eq. 2.5 are called the **Atomic Force Constants** . These are the derivatives of the force exerted on the atom the position lk because of the displacement of the atom at the l'k'position in the j direction, keeping all other atoms in equilibrium position.

Since the force on atom at the equilibrium position is zero

$$\Phi_{,i}(lk) = 0 \qquad (2.6)$$

Differentiating the harmonic terms in eq.(2.3) we get, by [7],

$$\sum_{l'k'} \Phi_{,ij}\ (lk;l'k')\ u_j(l'k') = F_i(lk,u) \qquad (2.7)$$

Eq 2.7 can be inverted using matrix mathematics and certain symmetry conditions to obtain the following relation which allows the calculation of the displacements undergone by the atoms

$$u_j(l'k') = \sum_{ilk} G_{ji}(l'k',lk)F_i(lk) \tag{2.8}$$

where the tensor G_{ji} is the inverse of the force constant matrix and is called the **Greens Function**. This tensor, like the atomic force constant, is a 3N by 3N matrix, and can be defined as the displacement of the atom at position lk in the j direction due to a unit force applied in the i direction on an atom at l'k' position. The derivation discussed above was developed by Maradudin et al [8].

2.1.2 Solution for Distortions around a Point Defect

The displacement of atoms in a crystal with a defect are larger in magnitude than the perfect lattice vibrations, therefore the harmonic approximation is no longer justified. The equilibrium equation of the form eq.(2.7) in the presence of a point defect then becomes

$$\sum_{l'k'} \Phi_{,ij}\,[lk;l'k']\; u_j[l'k'] = F_i[lk,u] - \sum_{l'k'} \Delta\Phi[lk;l'k']u_j[m'] \tag{2.9}$$

where the left hand side of the equation is simply the perfect lattice force constant matrix and the term on the right includes the defect force and the force contributed by the unharmonic terms in the potential expansion. The resultant term on the right is called the **Kansaki Force Matrix**, this matrix is characteristic of a defect. The inversion procedure used to calculate the displacements is very similar to that used for a perfect lattice.

$$u_j(l'k') = \sum_{lk} G_{ji}(lk,l'k')K_i(lk) \tag{2.10}$$

Here $K_i(lk)$ is the Kansaki force term. The 3N by 3N Greens function matrix could be reduced to N different 3 by 3 matrices [7], the calculation can be further simplified by using the symmetry of the lattice.

The short range Kansaki forces are usually estimated experimentally, by diffuse scattering, or Huang scattering techniques [9]. Computer routines have also been developed for point defect calculations using the Greens function technique [10].

2.1.3 Extension to Planar Defects

The procedure adopted to estimate the displacements of atoms beside the point defect can be used to obtain similar relations for stronger defects [11,12], such as, the planar defects. The accuracy of the experimentally estimated Kansaki force term is better when the measurements are done at positions that are relatively far from the defect. Therefore, the Kansaki force describes the effect of the defect on the atoms that are situated far from the defect. If the magnitude of the distortion caused by the defect is very large, the distortion as described by the Kansaki force would be very different from the actual behavior. Hence, an estimation of the displacements for planar defects is not very useful. In this section therefore, emphasis is placed on developing equations to understand the nature of oscillations that atoms would have undergone in the process of relaxation.

Consider two semi-infinite crystals that enclose a planar defect. In Figure (1). I and II are two semi-infinite crystals and m is the defect plane. If α and β are any two atoms, and the vector joining them is $\vec{x}_{\alpha\beta}$,

$$\vec{x}_{\alpha\beta} = \vec{R}_\beta - \vec{R}_\alpha$$

and the configurational energy of the whole system is given by,

$$\Phi(X) = \{\Phi_{\forall\beta\varepsilon I}(X_{\alpha\beta}) + \Phi_{\forall\beta\varepsilon II}(X_{\alpha\beta})\}_{\alpha\varepsilon I,\, II} \qquad (2.11)$$

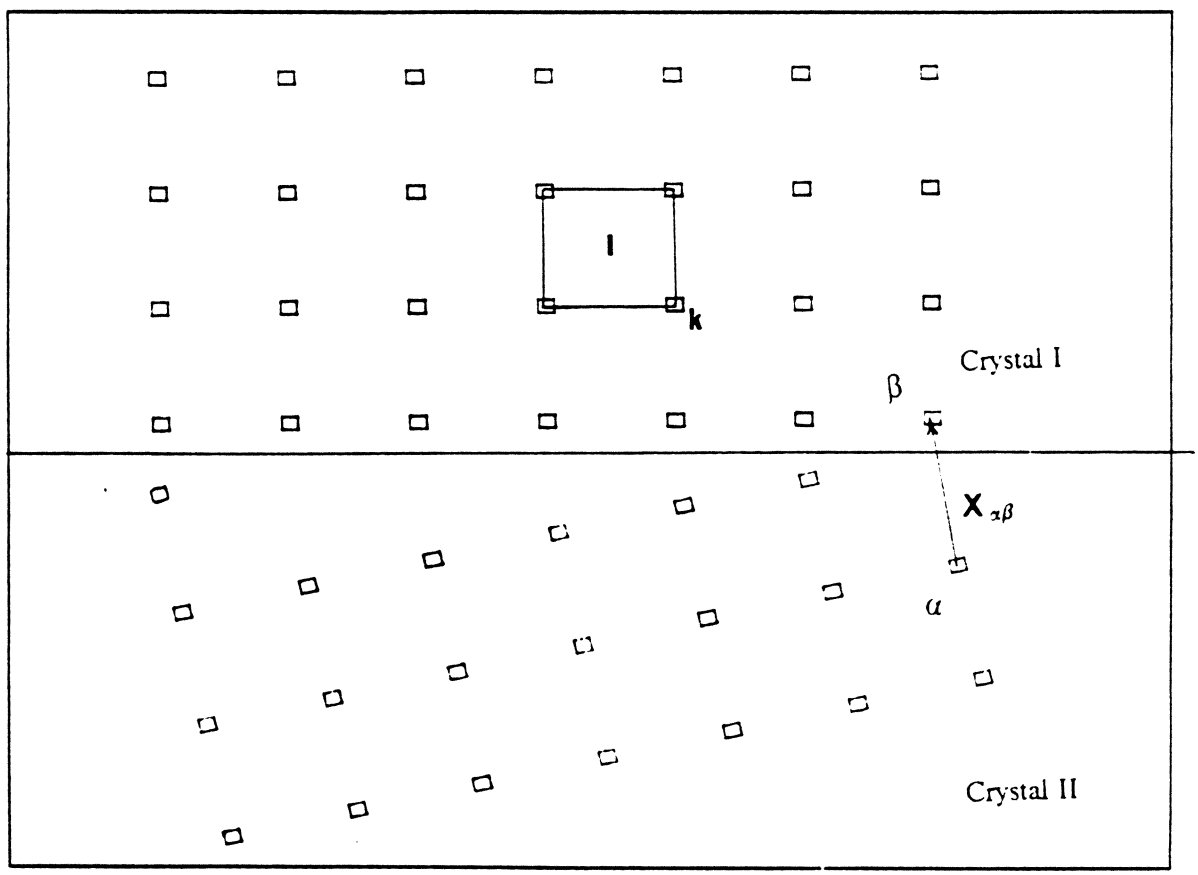

Figure 1. Atoms Around a Planar Defect

The Taylor series expansion (eq.(3)) modified to the present planar defect case can be written as,

$$\Phi - \Phi_o = -\sum_{lk} F_i^{I,II} u_i^I - F_i^{II,I} u_i^{II} + \frac{1}{2} \sum_{\substack{lk \\ l'k'}} \Phi^*_{,ij}(lk;l'k')\, u_i(lk)\, u_j(l'k') + \ldots\ldots \qquad (2.12)$$

where,

$F_i^{I,II}$ = the force on the atom I because of the presence of atom II.

The force on the atom in crystal space I because of the presence of atoms in space II is exactly the opposite of the force on atoms in space II. Therefore eq. (2.12) can be written as

$$\Phi - \Phi_o = -\sum_{lk} F_i[u_i^I - u_l^{II}] + \frac{1}{2} \sum_{\substack{lk \\ l'k'}} \Phi^*_{,ij}(lk;l'k')\, u_i(lk)\, u_j(l'k') + \ldots\ldots \qquad (2.13)$$

In the above expression also the unharmonic terms are neglected.

$\Phi^*_{,ij}[lk:l'k']$, is the defect force constant matrix. These coefficients can imagined to be a sum two different force constants,

$$\Phi^* = \Phi + \rho$$

where, Φ is the perfect lattice force constant as defined by the equation (2.7) and ρ is the matrix that exclusively describes the existence of the defect.

ρ is actually the sum of the forces on the atom due to the absence of atoms of same orientation and the presence of atoms of a different orientation.

$$\rho_{,ij}[l_I k_I : l_{II} k_{II}] = -\rho'_{,ij}[l_I k_I : l'_I k'_I] + \rho'_{,ij}[l_I k_I : l'_{II} k'_{II}] \qquad (2.14)$$

Where,

$l'_I k'_I$ = positions occupied by the atoms if the whole crystal were to be of orientation I.

Certain definite motifs can be identified in the Ni_3Al structure, (see section 4.1 for a detailed description). In order to understand the relaxation patterns, the forces and displacements undergone by the atoms are studied as two separate components eq.(2.15). First one is needed to describe the local relaxation within the motif while the other to account for the global relaxation around the defect. By analogy to the classical lattice relaxation modes, the global symmetric modes are called the acoustic modes, (F^0 and u^0), and the local antisymmeric components are referred to as the optical oscillations (F^Δ and u^Δ).

$$F(lk) = F^\circ(l) + F^\Delta(l)$$

$$u(lk) = u^\circ(l) + u^\Delta(lk) \tag{2.15}$$

$$F^\circ(l) = \frac{1}{N_k}\sum_k F(lx) \tag{2.16}$$

N_k = number of the number of non equivalent sites in the motif.

By the definition, the optical mode of forces do not extend beyond the motif in which they are present and they do not cause any resultant movement of the motif, hence,

$$\sum_k F^\Delta(lk) = 0 \tag{2.17}$$

When the optical and acoustic modes of forces and displacements are separated in equation (2.12) equation (2.18) is obtained

$$\Phi - \Phi_0 = -\sum_{lk}(F_i^{\circ} + F_i^{\Delta})(u_j^{\circ} + u_j^{\Delta}) + \frac{1}{2}\sum_{\substack{lk \\ l'k'}}\Phi_{,ij}(u_i^{\circ} + u_i^{\Delta})(u_j^{\circ} + u_j^{\Delta}) \tag{2.18}$$

To avoid complications, the dependence of the various parameters in the above equation on the position of the atoms, lk and l'k' are not mentioned.

By analogy to equation (2.6), the force on any atom at the equilibrium position is zero. Therefore,

$$\frac{\partial(\Phi - \Phi_o)}{\partial u^{\circ}} = 0$$

$$\frac{\partial(\Phi - \Phi_o)}{\partial u^{\Delta}} = 0 \tag{2.19}$$

By applying the equilibrium condition to equation (2.18) and simplifying the relation using the equations (2.16 and 2.17), we have,

$$N_k F^{\circ}(l) = \sum_{l'k'}\Phi_{,ij}(1 + 0)(u_j^{\circ} + u_j^{\Delta})$$

or when expanded,

$$N_k F^{\circ}(l) = \sum_{l'}\Phi_{,ij}(l{:}l')u_j^{\circ}(l') + \sum_{l'k'}\Phi_{,ij}(l{:}L'k')u_j^{\Delta}(l'k') \tag{2.20}$$

similarly for optical mode,

$$F^{\Delta}(l) = \sum_{l'k'}\Phi_{,ij}(l{:}l'k')u_j^{\Delta}(l'k') + \sum_{l'}\Phi_{,ij}(l{:}l')u_j^{\circ}(l') \tag{2.21}$$

The above equations describe the acoustic and optical modes of forces acting on the atoms. There are three (i= 1,2,3) acoustic equations which according to equation (2.20) describe the forces along the three perpendicular directions. And 3 ($N_k - 1$) optical equations, as described by equation (2.21).

The displacements in the first terms on the right of equations (2.20 and 2.21) correspond exactly to the nature of the force, the coupling between the two modes occurs in the second terms. This coupling can be made to cancel by choosing a weight factor for each atom type in the motif. However, in the present discussion a weight factor will not be used.

It is apparent from the above that the optical modes are caused by the micromoments within the motif and the acoustic mode describes the behavior of the motif as a whole.

2.2 Numerical Technique

Numerical relaxation techniques have been extensively used in the past to study grain boundary structures. There are well developed programs available that can be used to find the minimum energy structure of most defects. In this study the DEVIL code developed by Norgett et al.[4] was used to generate the lattice and relax the atoms around the defect. An atom is represented as a point in three dimensional lattice space and is allowed to interact with its neighboring atoms by a central pair interaction potential. A modified potential that includes a volume dependent term is used for the calculation. A detailed description of this is given in section 3 . The sum total of the force of interaction would be the energy of the ideal crystal. A computer routine that uses crystal symmetry was written to generate the different defects, the exact procedure used is described in chapter 5. The problem now is to relax the atoms situated around the defect. There are different techniques available to accomplish this. The static relaxation method is one where the atoms are assumed to have only potential energy given by eq.(3.6) and no kinetic energy. The conjugate gra-

dient method was used to perform the static relaxation and earlier this has been corrected to take care of the volume dependent potential.

Conjugate Gradient Method

In this relaxation procedure the atoms are moved from their initial position in a steepest gradient direction, i.e. the direction in which the rate of energy decrease is a maximum. The atoms are moved in this direction until the energy gradient is negative . Once the lowest energy position is attained the atoms are moved in a direction perpendicular to the initial direction of motion. This iterative procedure is carried out until no further energy lowering occurs by a movement in a perpendicular direction. The atoms can be moved in 3 N different directions.

This technique remembers the position of the atom after every relaxation and the next step of movement is carried out from the position reached as the result of the previous iteration; for this reason the convergence is fastest in this technique; in fact, it takes only 80 seconds of C.P.U. time, using the supercomputer at Virginia Tech., to handle 700 free atoms around a very strong defect as the grain boundary.

3.0 Interatomic Potentials

The necessary precursor for atomistic calculations in the present study is a detailed description of the atomic interactions. The central pair interaction potentials are the single most popular parameters for studying atomic interactions and consequently they are used in the present calculations.

3.1 Pair Interaction Potentials

A schematic diagram of a two body interatomic potential is shown in Figure (2). It consists of an attractive part at large separations approaching a minimum in the region of equilibrium separation, then becoming repulsive and rapidly rising as the interatomic separation decreases further. Estimation of such potential variation is not simple in many body systems. The interactions of a many body system is described by the equation below,

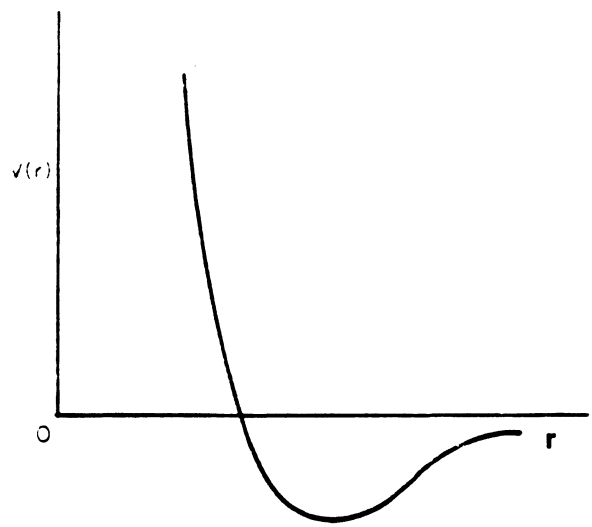

Figure 2. Schematic Potential for Two Body System

$$E = \frac{1}{2}\sum_{\substack{ij \\ i \neq j}} \Phi_{ij} \tag{3.1}$$

where Φ_{ij} is the potential value for a particular interaction. If theoretical potentials are used for calculation of many atom interaction, the results deviate considerably from the actually observed behavior. Therefore empirical potentials were used here. Empirical potentials are based on simple analytical expressions that may or may not be theoretically justifiable, the parameters in the expression are adjusted such that certain measured data are fitted to the potential. The application of computer techniques to these problems have permitted the use of complicated potentials which are based on many experimental parameters. Most empirical potentials fit to a set of experimental constants with the choice often based on the interests of the investigator. For this reason there tends to be some doubt in the results obtained from empirical potentials. Every potential developed is fitted to essential constants such as the lattice parameter and the cohesive energy.

The first few models that were employed to calculate the atomic interactions using the pair interaction potential method are the Lennard Jones potential and the Morse potential.

Lennard Jones potential

The general form of the Lennard Jones potential [13] is described by

$$\Phi_{ij} = -\frac{A}{r_{ij}^4} + \frac{B}{r_{ij}^4} \tag{3.2}$$

The description of the Lennard Jones potential relies on the fact that the attractive and repulsive forces acting on the atom depends on the distance of separation of the atoms. For alloys like Ni_3Al this simple description needs only six constants to be determined, these can be estimated easily from the physical constants and experimental results obtained the diffraction data for example.

In contrast the Morse potential [13] depends exclusively on the power law. This potential can be written in the form

$$\Phi(r) = D e^{-2\alpha(r - r_o)} - 2 D e^{-\alpha(r - r_o)} \tag{3.3}$$

The Morse potential is developed to satisfy the following conditions :

- $\Phi(r) \rightarrow 0$ as $r \rightarrow \infty$
- $\Phi(r)$ is minimum when $r = r_o$ [3]
- $\Phi(r) \rightarrow \infty$ as $r \rightarrow 0$

Here again the parameters D and α are calculated so as to fit the essential constants of the material.

An accurate model is expected to predict the long range elastic properties of the material. The simple models described above do not take into account the many body interactions and therefore fail to produce the elastic properties of the material. Hence, we need a more exhaustive model for our defect studies.

3.1.1 Potentials for Alloys

A large number of interatomic potentials are available for many commercially used pure metals. However , the choice is much more limited in case of alloys. There are examples of potentials that have been developed for alloys [14-15], but very few these have been used for defect calculations. A very successful scheme of potential estimation has however been developed for the first time by Machlin [16-18]. In his scheme the potentials for pure components A and B, in alloy AB were determined by the regular procedure of estimation of potentials. The average of both

[3] r_o is the first neighbor distance

potentials for pure A and pure B is taken as the potential of the alloy. The corrections required to fit the lattice parameter, cohesive energy and charge transfer are included as a separate term in the expression for the potential. The inherent problem associated with this method of potential determination is the absence of volume dependence terms in the determination of the potential. It is very difficult to express the cohesive energy exclusively in a pairwise term alone, this is particularly true in metals where most of the cohesion is brought by an electron cloud.

3.2 Volume Dependent Potentials

Madea et al [19] proposed a procedure analogous to the scheme developed by Machlin. Here the potential expression, for pure A and Pure B , has an explicit volume term as shown in equation (3.4)

$$E^A = \frac{1}{2}\sum_{i \neq j}^{N} \Phi^A(r_{ij}) + U_v^A(v) \qquad (3.4)$$

Where,

E^A = total energy of the ensemble of atoms of type A

$U_v^A(V)$ = volume dependent term

The volume dependent term is believed to contribute to the cohesive energy. The disturbance in the density of the atoms is usually found in the vicinity of a strong defect, and is taken care of by the volume dependent term. The disadvantage of this procedure of estimation is the failure of these potentials to describe the interaction of atoms that are exposed to different volume. In the potentials that were used in this study, this problem was overcome by implicitly including the volume term. The improved potentials used here have a built-in volume dependence of the form

$$E = \sum_i E_i$$

$$E_i = \frac{1}{2}\sum_{j \neq i} \Phi(r_{ij}) + F \sum_{j \neq i} \rho(r_{ij}) \qquad (3.5)$$

Where,

$\rho(r_{ij})$ = volume density about each atom

it is a measure of crowding about the atom.

The cohesion here rises as a consequence of both the pair wise term and the volume dependent term on the right hand side of the equation.

Embedded Atom Method

Recently another scheme has been developed for potential estimation using the principle of volume dependent potentials. This is the so called 'Embedded Atom Technique' [20]. According to this model the major component of the alloy is treated as the 'host atom' and the alloying element as the embedded impurity atom. The total energy of the system is described by separate terms. as shown below,

$$E_{embd} = \sum_i F_i(\rho) + \sum_{ij} E_{ij}^{cl} \qquad (3.6)$$

Where,

ρ = density of the atom nucleus

E^{cl} = Classical electrostatic interaction between atom and electron.

$F_i(\rho)$ = energy due to placing an atom at position i

in a background element of electron density ρ at i.

The function $F(\rho)$ takes care of all the quantum mechanical interactions between the atom and the host electron density. The classical electrostatic interaction is given by equation (3.7).

$$\Phi_{ij}(r) = E^{cl} = Z_i\frac{Z_j}{r} - Z_i\int Z_j\rho_i(r)\frac{dr}{|r-r_j|} - Z_j\int Z_i\rho_j(r)\frac{dr}{|r-r_j|} + \int\frac{\rho_i\rho_j Z_i Z_j dr_1 dr_2}{|r_1-r_2|} \quad (3.7)$$

The negative terms in the expression above is due to the attraction of the nucleus and the electrons and the positive terms represent the electron electron and the nucleus nucleus repulsions.

Where,

$$Z_i = Z_{io}e^{-a_i r}$$

here:

Z_{io} = effective atomic number of atom i

a_i = screening constant for atom i

The choice of the screening constant is the matter of convenience. The potential calculated using the above expression has the following properties. The function $\Phi(r)$ is attractive at all neighbor distances, and the volume dependent F (ρ) provides the repulsion. The potentials used in this study were developed at the Los Alamos National Laboratory in New Mexico [21]. The procedure adopted in the calculation of the potentials for Ni_3Al using the embedded atom method is:

1. The Nickel and the Aluminum potentials are estimated by the technique described above. The embedded and the host atom are the same for the pure materials. The screening function and the volume dependent function are chosen such that the crystal energy as a function of the

lattice constant matches the universal form given by Rose et al [22]. This leads to excellent agreement with the experimental values of lattice constant, cohesive energy and bulk modulus [25].

2. Without altering the Nickel and Aluminum fits, the Ni-Al cross potential (pair potential term) is determined by optimizing the fit to certain constants that are listed here.

   Lattice parameter

   Cohesive energy of Ni_3Al, NiAl

   Elastic constants

   Super intrinsic stacking fault energy

   Anti phase boundary energy

   Ordering energy

   Vacancy formation energy.

3.3 Limitations

1. Since many different types of potentials with each fitted to a certain set of measured quantities are available, it becomes difficult to choose the one that would best serve a particular problem.

2. The validity of the potential used is not established in the presence of a defect. The behavior of the potentials could well be altered in the presence of a vacancy or a surface termination. The static defect calculations are rather potential sensitive. In general, therefore , the interesting and accepted results of computer simulation are not the absolute numerical values for a given quantity but the comparative values of two or more quantities.

3. The role played by thermal vibrations cannot be included in the potential calculations, the structure and kinetics of the defects are reasonably dependent on the thermal activation.

Provided that a certain amount of caution is exercised in interpreting the results obtained from computer simulation, there is no reason why these potentials cannot be employed with considerable success to improve the present understanding of the problem involving atomic motion in crystals.

4.0 Structural Considerations

4.1 Crystal Structure of Ni_3Al

When an alien atom is introduced into a host lattice, the added atom could occupy any of a number of lattice positions. In such a case a random distribution of the different atoms is often observed for alloys. Ordered alloys are certain specific cases where the atoms of a particular kind have a higher probability to occupy certain specific sites in the lattice. Therefore, the resultant lattice structure could be imagined as two different lattices interpenetrating into each other, this type of lattice is called a superlattice.

The ordered Ni_3Al alloy has a so called '$L1_2$ Super Lattice structure', The $L1_2$ structure is very similar to the f.c.c. structure. A f.c.c. cell with Nickel atoms in the face center positions and Aluminum atoms at the cube edge positions can be thought of as the Ni_3Al structure , (see Figure (3).) Some researchers also describe the $L1_2$ structure as a simple cubic type where the s.c. lattice is formed by the repetition of a motif. A motif is an aggregate of four different atoms each of which belong to a certain sublattice. It is easy to realize that if three face center positions and a cube edge position is treated as a single lattice point then the f.c.c. cell could be treated as a simple cubic lattice.

4.2 *Grain Boundary Structure*

Research on grain boundaries has been so extensive that there are many theories to explain the grain boundary structure. These models are so well advanced that they can explain quite a few of the observed kinetic and mechanical properties of the boundary.

Most geometrical models describe the grain boundary as an interface created at the plane of intersection of two crystals that are mismatched because of a misorientation or a mis-translation. The terminology used commonly in grain boundary classification includes :

Tilt boundary

When the axis of rotation that defines the misorientation between two crystals is in the plane of the boundary, the grain boundary is called a tilt boundary. The geometry of formation of a tilt boundary involves a relative rotation of the two crystals, which can be brought about by cutting a wedge from a perfect crystal. This is equivalent to an array of edge dislocations of the same Burger's vector in a crystal [26]. The **Symmetric tilt boundary** is a special case of this boundary where the grain boundary plane bisects the angle of misorientation. The grain boundaries generated in this study were of the symmetric tilt type. Over the years, theoretical calculations based on these type of boundaries have been proved to be very successful [35]. The tilt angle or the misorientation angle is the angle between a particular family of planes in the two crystals intersecting to form a boundary.

Twist boundary

The class of boundaries whose rotation axis is perpendicular to the boundary plane are called the twist boundaries. A simple example of a twist boundary is the interface formed from a cross grid of pure screw dislocations. A single set of parallel screw dislocations has a long range

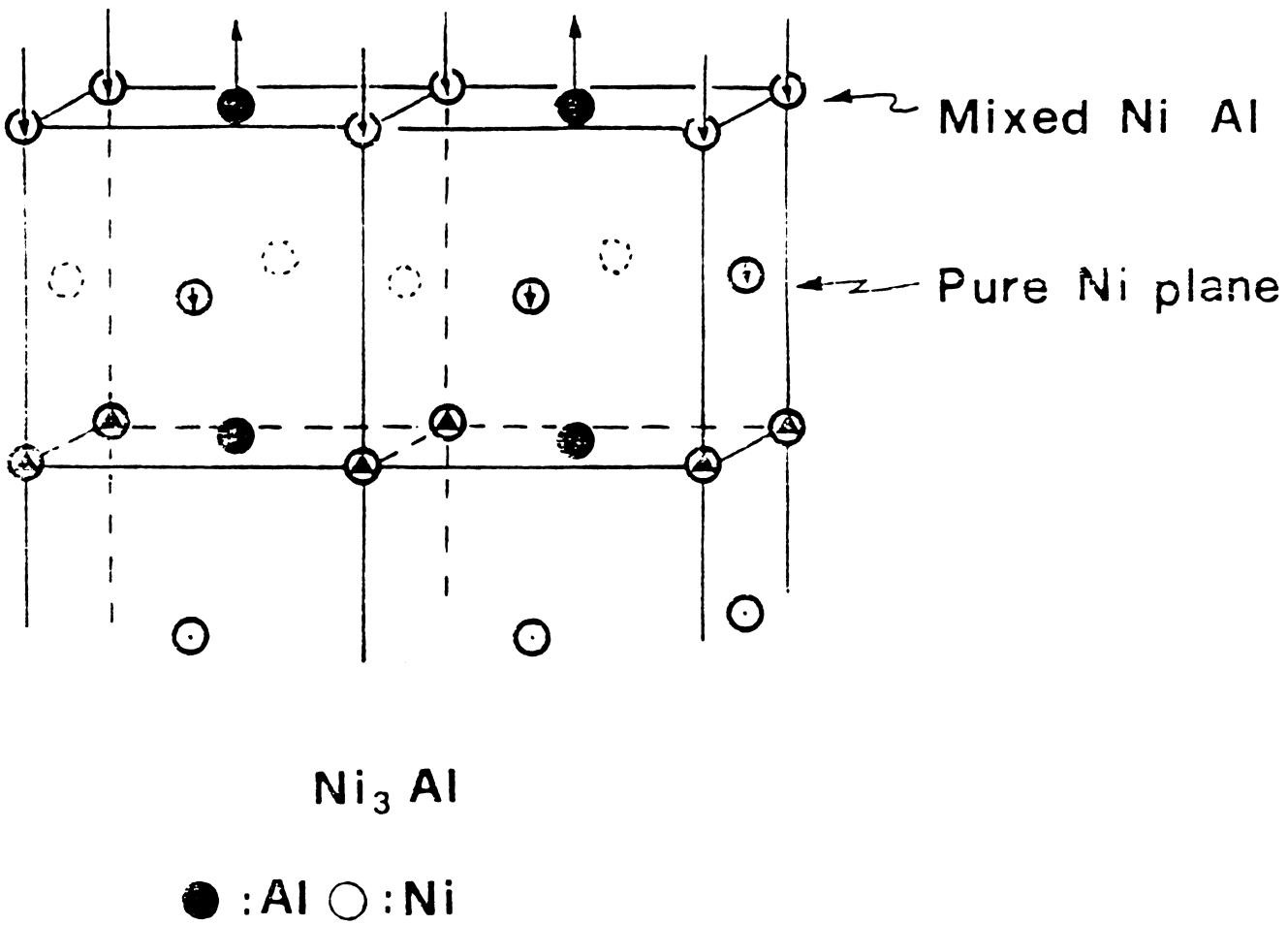

Figure 3. Crystal Structure of Ni_3Al: showing the four sublattices from reference [22].

stress field but is cancelled by a second set of screw dislocations placed perpendicular to the initial set [27].

4.2.1 Coincidence Site Lattice Boundaries

The coincidence site lattice (C.S.L.) model is a well established geometric model used to study the grain boundary structure. The main reason for its popularity in this field is the simplicity involved in comprehension and calculation of these types of boundaries. The coincidence site lattice concept can most easily be understood by imagining two crystals lattice at some relative misorientation which interpenetrate. If we let a lattice point from each crystal to be brought into coincidence by relative rotation, at certain relative orientations called the **'Coincidence Orientations'**, a three dimensional lattice of coincidence of crystal lattice points exists, which is known as the coincidence site lattice. The reciprocal density of the coincidence sites relative to the crystal lattice site is denoted by Σ and is used to characterize different coincidence boundaries. $\Sigma = 5$ would imply that one in every five atoms of one lattices coincides with the atoms of the lattice on the other side of the boundary. Figure(4) shows two interpenetrating f.c.c lattices, the coincidence sites can be clearly seen to be one fifth of the total number of lattice sites, hence this is a $\Sigma = 5$ boundary. The misorientation angle for this boundary is 36 °87′, circles and squares denote atoms on two successive [002] planes projected about [001]. From the definition of Σ it is obvious that the low Σ boundaries have more coincident sites and $\Sigma = 1$ would imply an absence of any boundary.

It is also interesting to note that certain repeating **structural units** can be identified at the grain boundary. A structural unit is defined as a small group of atoms arranged in a characteristic configuration. The size of this repeating structural unit has been found to be dependent [25] upon the Σ value for the boundary with low Σ boundaries having smaller structural units.

The statistical occurrence of certain boundaries have been found to be more frequent than others [25,28,29] and these are called favored boundaries or special boundaries. The properties

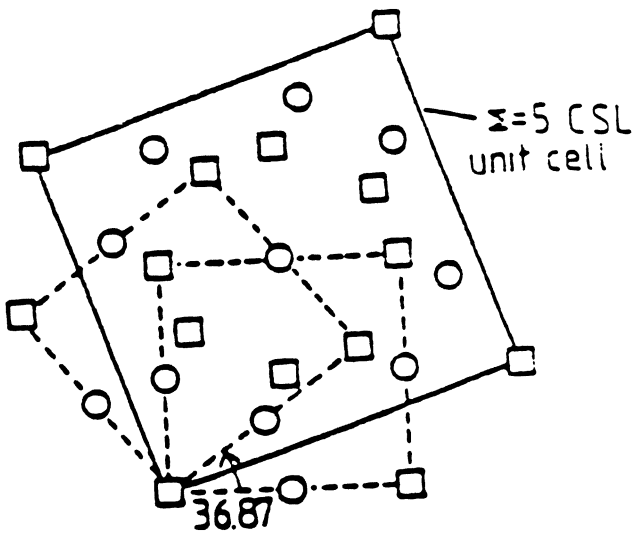

Figure 4. Coincidence Site Lattice Model
: from reference [20]

Page 29
is missing from all
copies of this piece

Based on their experimental analysis Straumul et al.[30] have found that for quite a few grain boundary misorientations the properties of the boundary are retained even at relatively high temperatures, roughly 0.65 Tm. [4] Interestingly enough, $\Sigma = 5$ is an example of such a special boundary. This is possible because the crystallinity of these boundaries are retained even at high temperatures [30]. Therefore it quite reasonable to study this boundary with a theoretical model that is based purely on crystalline geometry, such as ours.

It is fairly obvious that three nonequivalent structures of the $\Sigma = 5$ boundary are different from each other simply because of the presence or absence of an extra (210) plane. In a recent study it has been shown that at non zero temperatures a structural transformation from one boundary structure to another could take place and the vacancy concentration plays an important role in such transformations [35]. This is also true in case of high Σ boundaries where the repeat units can be defined by a certain combination of delimiting boundaries. There is evidence, based on certain diffusion experiments, of such structural transformation in the $\Sigma = 5$ near coincidence boundary of copper and has been identified at high temperatures [34]. However, it is difficult to predict such behavior in Ni_3Al, since the effect of temperature is difficult to study in such simulations. Consequently it is not possible to probe into this type of transformation.

[4] Tm is the melting temperature

5.0 Computational procedure

The primary aim of this study is to understand the structure of the planar crystal defect interfaces and relate them to the observed properties. A FORTRAN program that uses the DEVIL code is used to simulate these interfaces [4].

The potentials used in this program are fully empirical and were developed at the Los Alamos national laboratory [21]. Using a set of potentials for Ni_3Al it is possible to generate the pure Al and pure Ni lattices since the potentials of the alloys are simply the corrected average of the potentials of its constituents. The corrections of the potential to fit the constants of the alloy are included as a separate cross potential Φ_{AB} term, and hence do not affect the Φ_A or Φ_B potentials.

The computer program can generate any cubic crystal lattice, the lattice to be generated is defined by stating the atom positions in the unit-cell. For example the f.c.c cell is generated by giving the atom position as (0,0,0), $(0,\frac{1}{2},\frac{1}{2})$ type. Once the required lattice type and the lattice parameter are given the program generates a parallelopiped of atoms which are bound by three mutually perpendicular planes whose normals are along the three cartesan directions x, y and z. As mentioned earlier, the crystal structure of Ni_3Al is of the $L1_2$ superlattice type, which is simply the f.c.c lattice with Nickel atoms in the face-center positions and the Aluminum atoms at the cube

edge positions. This lattice can be generated as a f.c.c lattice with different atoms at the face-center position and the cube edge positions.

The atoms that are along the edge of the parallelopiped do not have the required number of nearest neighbors, therefore they would loose some interactions if they are relaxed as such. To overcome this problem an outer block of atoms are generated, (Region II in figure(5)). The atoms in Region I in the figure are free to move under the influence of the potential while the atoms in Region II are treated to satisfy the long range elastic interactions of the defect.

The accuracy of the result obtained from these calculation seem to depend directly on the number of atoms that are allowed to interact. The number of atoms that the program can take is limited by the computer processing time. A cyclic repetition of the initial parallelopiped of atoms would considerably increase the number of atoms used for relaxation without affecting the computer processing time much. The location S of an atom M situated in the cyclically repeated region is uniquely related to the atom, M^o, with in the initial block, by the relation (5.1)

$$S[M] = S[M^o] + m\,\delta x\vec{x} + n\delta y\vec{y} + o\delta z\vec{z} \qquad (5.1)$$

where :

m,n, o are integers

$\delta x, \delta y, \delta z$ are the periodic lengths

Hence it is apparent that the displacement of atoms is equal

$$U[M^o] = U[M] \qquad (5.2)$$

Since the coordinates and the displacements of the cyclically repeated atoms are similar to the ones in the initial block the processing time is not increased by the inclusion of cyclic atoms.

To study a point defect one can employ cyclic boundary conditions in all three directions $\vec{x}$, $\vec{y}$ and $\vec{z}$. Whereas, to study a planar defect such as a stacking fault or a grain boundary a cyclic boundary condition in a direction perpendicular to the defect plane would repeat the defect, which is undesirable. In the present study such defects are generated in a plane containing the $\vec{x}$, $\vec{y}$ directions and so no repetitive boundary conditions are used in the $\vec{z}$ direction.

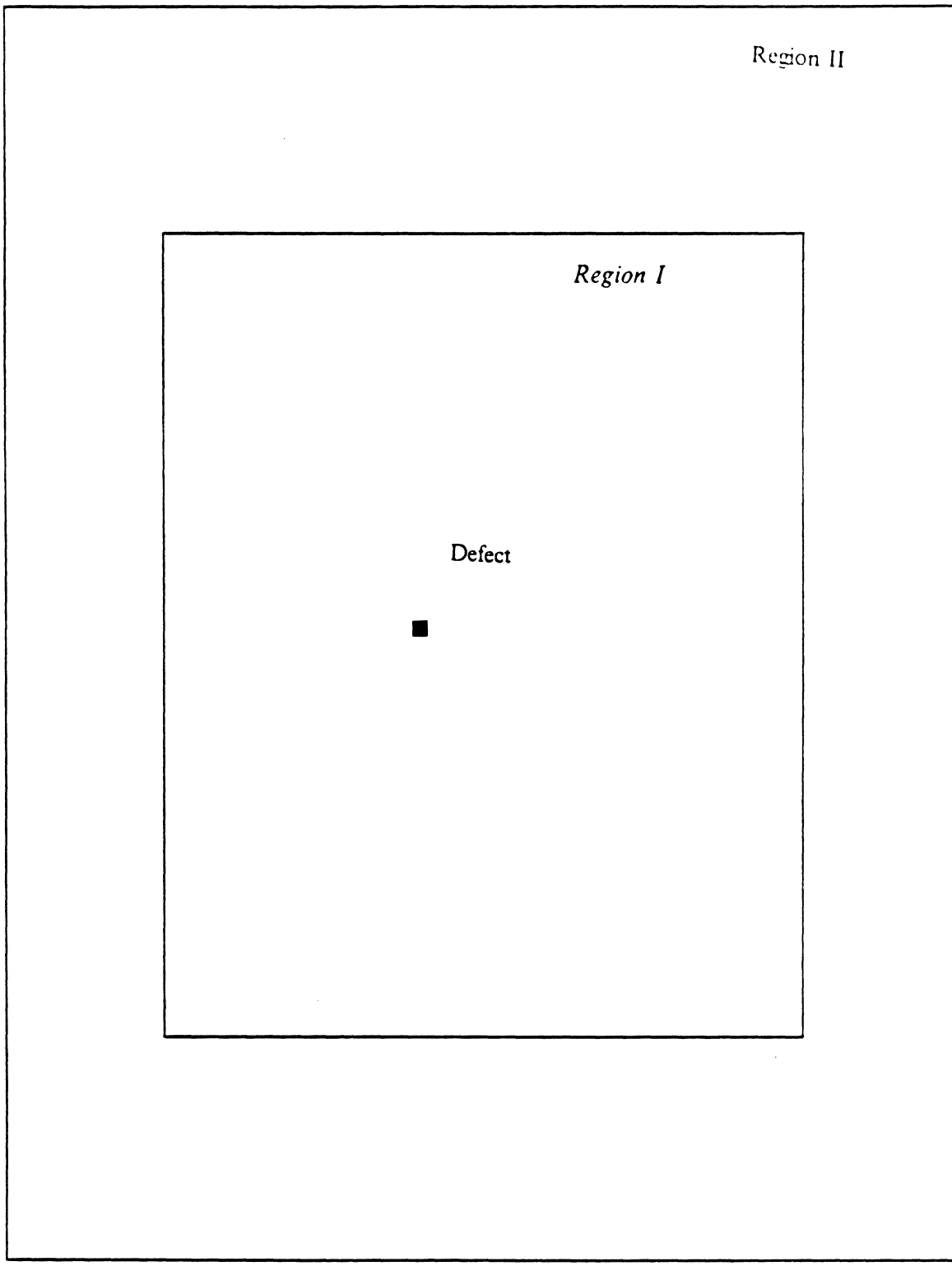

Figure 5. Regions generated by the Program

5.1 Generation of Defects

5.1.1 Vacancy

Absence of an atom at its lattice site is termed a vacancy. To simulate the effect of a vacancy in this program, the atom at the site where the vacancy is to be created is removed. Similarly an interstitial can be generated by including an atom in a suitable interstitial position. When a lattice is cyclically repeated with a vacancy the vacancy is also repeated. To ensure that the vacancies do not interact with each other, the δ x, δy, δz are chosen large enough to accommodate the distortion within each block.

5.1.2 Twin

The planes binding the block of atoms are chosen in such a way that the twin plane is one of the edges of the parallelopiped. In this study to generate a (111) twin, [111] , [11-2] , [1-10] were used as the Cartesian directions. The twin is generated simply by reflecting the lattice around a reference (111) plane. The defect plane is extended by cyclically repeating the lattice in the [11-2],the $\vec{x}$ and [1-10], the $\vec{y}$ directions. The displacements of the atoms along the three orthogonal directions can then be obtained from the program and plotted as a function of the position of the atoms in order to study the displacement field around the defect. The number of planes in the $\vec{z}$ direction, δz , were chosen such that the atoms in Region II do not restrict the distortions created by the twin.

5.1.3 Stacking Fault

Stacking faults are of two types, extrinsic faults and intrinsic faults. The extrinsic fault is one where an A B C A C B A B C [5] type of stacking is found as a result of the fault.Since the extrinsic stacking fault generates two sequential errors in the stacking sequence, it is sometimes referred to as the 'double fault'. The intrinsic fault is characterized by a A B C B A B C A stacking sequence. The energy required to create a double fault is twice the one required to generate an intrinsic fault, consequently we do not observe many extrinsic faults in crystals. For this reason, for the present calculation only intrinsic stacking faults were used. The faults are introduced by displacing the atoms through the stacking fault vector for all atoms above the plane of the defect The stacking fault vector in f.c.c is

$$\vec{S} = \frac{1}{6}[211] \tag{5.3}$$

Figure (6) shows a plane of (111) in f.c.c with the stacking fault vector, $\vec{S}$. To shift a B type plane to a C type one, a displacement in the [11-2] direction of magnitude,

$$|S| = \frac{a}{\sqrt{6}} \tag{5.4}$$

was given.

In the $L1_2$ structure a displacement of atoms through the S vector would cause an anti-phase boundary. To place a Nickel atom over another Nickel atom after displacement, a displacement of twice the magnitude as given by equation (5.4) is required. Therefore the fault vector in $L1_2$ superlattice is

$$\vec{SS} = \frac{1}{3}[211] \tag{5.5}$$

---

[5] the fault is shown underlined

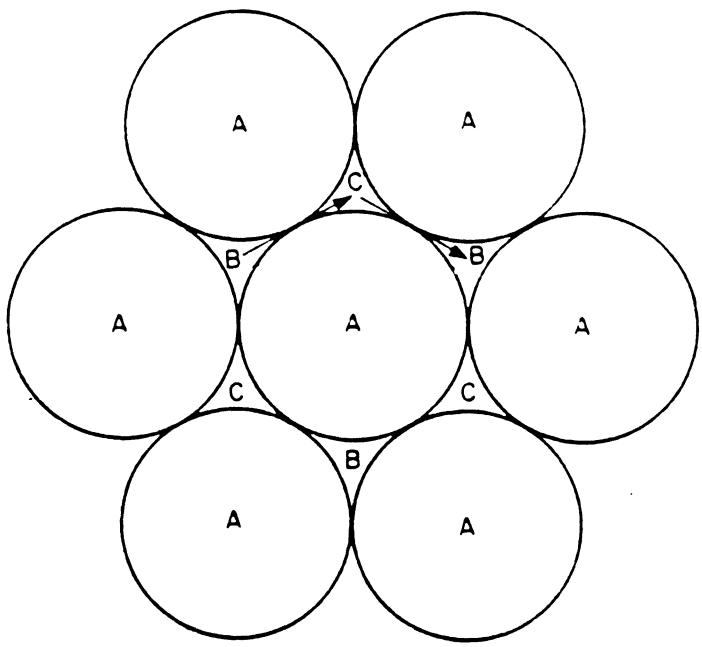

Figure 6. Stacking Fault Vector in f.c.c.

Table 1. The Translations for the stacking fault along [211].

	Ni	Al	Ni_3Al
Lattice parameter in Å	3.52	4.025	3.573
Stacking Fault $\vec{S}$ in Å	1.437	1.643	2.9173

This vector is called the **Super lattice intrinsic stacking fault** vector. The number of planes used to relax the atoms has a large bearing on the results of these simulations, if an insufficient number of planes are used in the non-cyclic direction then the energy obtained would be inaccurate, since the constraints induced by atoms of Region II would create a sharp jump in the displacement gradient. Table 1 shows the magnitude and direction required to generate a stacking fault in the three materials, Nickel, Aluminum and Ni_3Al. The same set of orthogonal planes that was used to generate the twin was also used for stacking fault.

5.1.4 Antiphase Boundary

The boundary that separates the domains in the ordered alloy with a superlattice structure is the anti-phase boundary. Each domain in such alloys represent a particular kind of ordering or disordering. In the $L1_2$ ordered alloy two different antiphase vectors are permissible. The procedure adopted to generate this boundary is exactly similar to to the one for stacking fault, except that the magnitude of the translation given is equal to that of the anti-phase vector, $\vec{A}$.

1. $\vec{A} = \frac{1}{2}[110]$

2. $\vec{A} = \frac{1}{6}[211]$

In this study the 1/6[211] vector is used. Electron microscopy studies of $L1_2$superalloys have revealed the the existence of such antiphase boundaries in a tubular form [36]. In Ni7sub3.Al a large density of tubes lying along $< 110 >$ directions have been observed [37].

5.1.5 Surfaces

Any termination of a regular array of atoms can be called a surface. The program used in the present can also be used to generate such a surface on any one of the bounding planes of the parallelopiped. All lattice positions are set to be vacancies above a certain reference plane and this is equivalent to generating a surface that terminates at the reference plane.

5.1.6 Grain Boundaries

The C.S.L boundaries with $\Sigma = 5$ were generated, these are special tilt boundaries that have a structure which is very similar to a twin boundary. The Ni_3Al lattice is generated with the (210) plane as one of the binding planes of the block. The other orthogonal planes used were the (1-20) and (001). The boundary is created by reflecting all the atoms above the grain boundary to their respective positions below the boundary. The lattice on one side of the boundary is an exact mirror image of the other. The line of intersection of a particular family of planes of the two different crystals on the grain boundary plane is the tilt axis. This type of reflection of the lattice would cause certain atom centers to be as close as 0.4 a [6] Atoms that are so close would cause an exponential rise in the energy of the system. Since the program cannot handle such large disturbances, one of the pair of atoms that were as close as 0.4 a was voluntarily removed before the relaxation procedure.

---

[6] . a is the lattice parameter

5.2 *Defect Interactions*

Materials used in practice are bound to have many defects in them. Therefore, to get a good understanding of the effect of atomic structures on the properties of the material one needs to conduct simulations with many defects.

Using this simulation it is possible to introduce as many defects as desired in the lattice, but the results obtained from such studies will not be useful unless one uses an infinitely large number of atoms. When more than one defect is present in the crystal the planar symmetry of the defect is lost and therefore we lose the luxury of using cyclic boundary conditions. Convergence is much faster with the cyclic boundary conditions since the lattices is essentially comprised of a unit that repeats itself. Yet, there have been examples in the past were an interaction of two defects have been studied. For example, Crocker et al [38] studied the vacancy interaction with the grain boundary in certain commercial metals such as copper and iron. In the present work interaction of the vacancy with the $\Sigma = 5$ (210) [100] boundary was studied. A block with the grain boundary and the vacancy was generated and cyclic boundary conditions were employed to repeat the boundary plane. This procedure would generate infinite number of vacancies. Enough care was taken to ensure that these vacancies do not interact with each other. The number of atoms in the repeating block was increased such that the disturbance caused by the vacancy dies down within the same block.

5.3 *Rigid Body Translation*

Rigid body translation is defined as the movement of one crystal as a whole, with respect to the other crystal enclosing the defect. It is well established that an optimum rigid body translation of one crystal relative to the other which contains the defect, reduces the energy of the

defect. The optimum rigid body translation required in each orthogonal direction was identified by studying the behavior of displacement field in the vicinity of the defect. The rigid body translation thus calculated was accomplished in the simulation by shearing one crystal through this distance while retaining the other crystal stationary.

5.4 Energy Minimization Procedure

Various steps involved in the energy relaxation procedure are described here. Though, some of these functions were explained in detail earlier, they are mentioned here to provide an idea of the sequence of various operations.

1. A perfect lattice of the given crystal structure, atom positions and atom type is generated by the computer routine. Orientation of the lattice being determined by the choice of the $\vec{x}, \vec{y}$ and $\vec{z}$ directions.

2. The potential values are assigned to each atom and a list of atoms that interact with a particular atom is created. This list is called the 'look up list' the number of neighbors that an atom is permitted to interact with is controlled by the user. A parameter called the **radius of lookup** is used to obtain different neighbor interactions.

3. The sum total of the energy of all the aforementioned interactions is estimated, and this energy is termed the unrelaxed energy of the lattice. In the next step, the conjugate gradient technique (discussed in section 2.2) is used to obtain the relaxed configuration. In order to obtain the lowest energy structure using the conjugate gradient technique the atoms are moved to the lowest possible energy configuration in many different directions.

4. The lattice is then regenerated with the defect and steps two and three are repeated. Apart from the energies, the displacements undergone by the atoms in the process of relaxation, the force on each atom, e.t.c. can be obtained as output from the program.

6.0 Simulation Results

The results obtained for the defect calculations carried out for various planar defects in the present study in Ni_3Al were presented at the Gorden conference on Physical Metallurgy, New Hampshire, 1987, [39]. Apart from these results, additional results were obtained for the simulation of vacancy interactions with the grain boundary. Furthermore some surface studies are presented in this chapter.

An interesting result that was first identified from the computer simulation work was the presence of a rigid body translation between the two halves of a defected crystal [38]. The lowest energy defect structures obtained in this study were also found to show a rigid body translation in the direction perpendicular and or parallel to the defect plane. The values of these rigid body translations are given in Table 2.

The various defect energies obtained here correspond with the values reported in literature and this fact corroborates the validity of the model. Almost all defects studied appear to displace the atoms around them in all three directions x, y, z. However, the displacements in the x and y directions (directions contained in the plane of the defect) are of a lesser magnitude than the displacements in the perpendicular direction. As expected, the atoms close to a defect undergo a considerably larger displacement relative to the ones far from the defect. The magnitude of the largest displacement undergone by any atom is found to depend on the strength of the defect. There

Table 2. Simulation Results of (111) Planar Defects

Defect	Rigid Body Displ. in units of (a)	Acoustic Mode	Optical Mode	Energy mJ/m^2
Twin Ni_3Al	-.006	[111]	all directions	12
S.I.S.F Ni_3Al	-.006	[111]	all directions	13
A.P.B. Ni_3Al	0	[111] [112]	all directions	142
Surface Ni_3Al	--	[111]	all directions	1,700
Twin, Ni	+.0056	[111]	--	29
Twin, Al	+.0163	[111]	--	46
Stacking Fault, Ni	+.006	[111]	--	59
Stacking Fault, Al	+.02	[111]	--	81

is a direct correlation between the formation energy of the defect and the severity of the distortion caused by the defect. Distortions generated by the defect were studied by observing the displacement undergone by the atoms as a function of there position relative to the defect. The results obtained for different defects are presented here.

6.1 Twin

The (111) twin happens to be the planar defect with the lowest formation energy possible. The simplicity involved in the defect configuration helps one to observe all the oscillation modes in this defect. Crocker et al [33] found that in certain commercial metals like copper an iron the (111) twin wound need a rigid body translation in a direction perpendicular to the defect plane. Similar results were obtained for Nickel, Aluminum and Ni_3Al. The values of the rigid body translation required to achieve the minimum energy configuration are given in Table 2. The twin in Ni_3Al causes the twinned crystal to come closer to the untwinned one by .006 a, [7] this is in contrast to the rigid body repulsion seen in the pure components Ni and Al

In Table 2. the rigid body translations are represented as the ratio of their corresponding lattice parameters. As explained earlier, the relative values obtained from numerical calculations using pair interaction potentials are of more interest than the absolute value. A representation of this sort would facilitate the comparative analysis.

In Figures(7,8 and 9) the displacements of the atoms along the z direction are plotted as a function of their distances from the boundary plane. The atoms in the upper half of the crystal (ones with positive distance from the boundary) are twinned with respect to the bottom crystal. Figures (7 and 8) for pure Aluminum and Nickel respectively, show a symmetric displacement of

[7] a is the lattice parameter

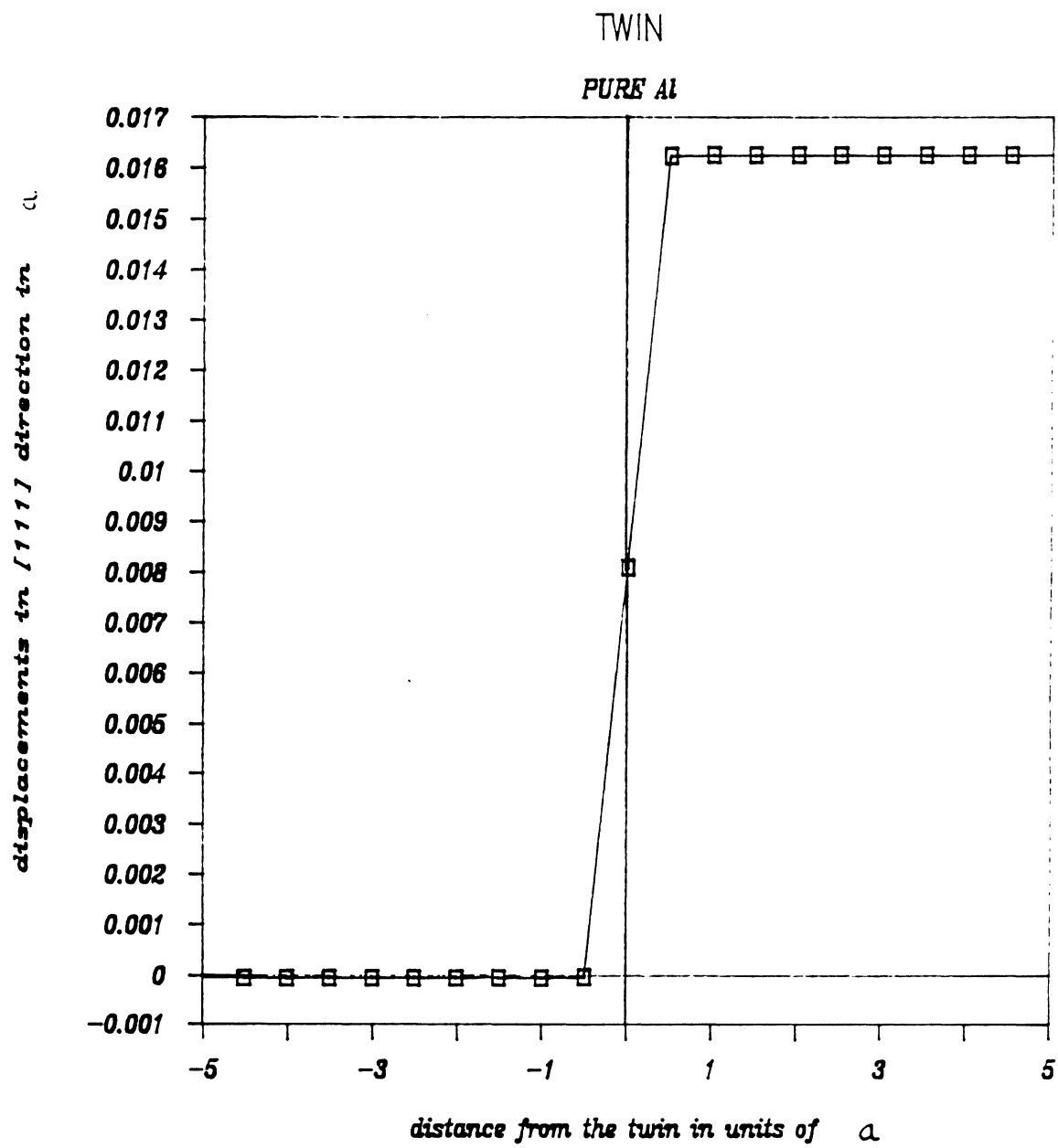

Figure 7. [111] Displacements of Atoms In Aluminum Away From (111) Twin

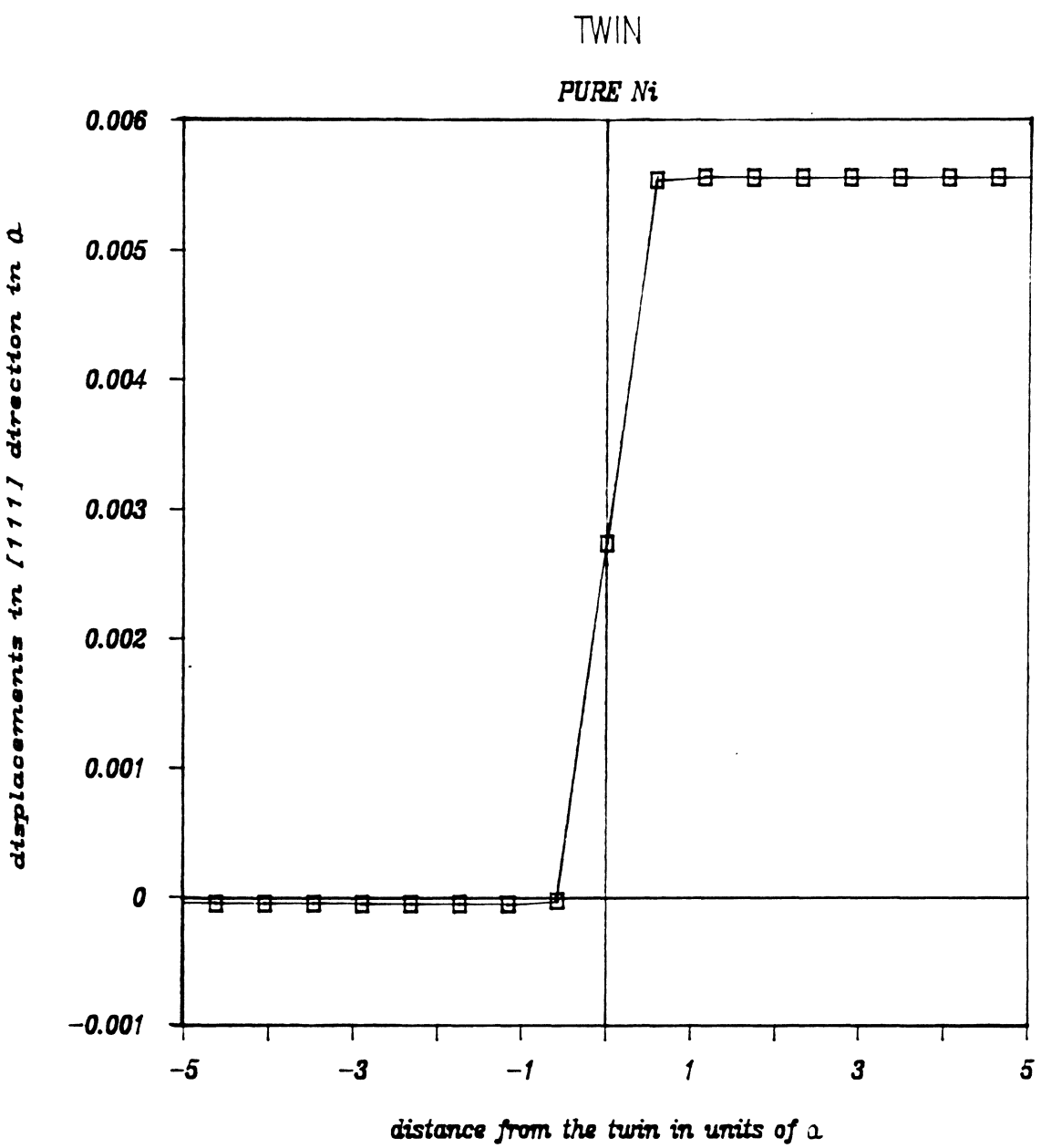

Figure 8. [111] Displacements of Atoms In Nickel Away From (111) Twin

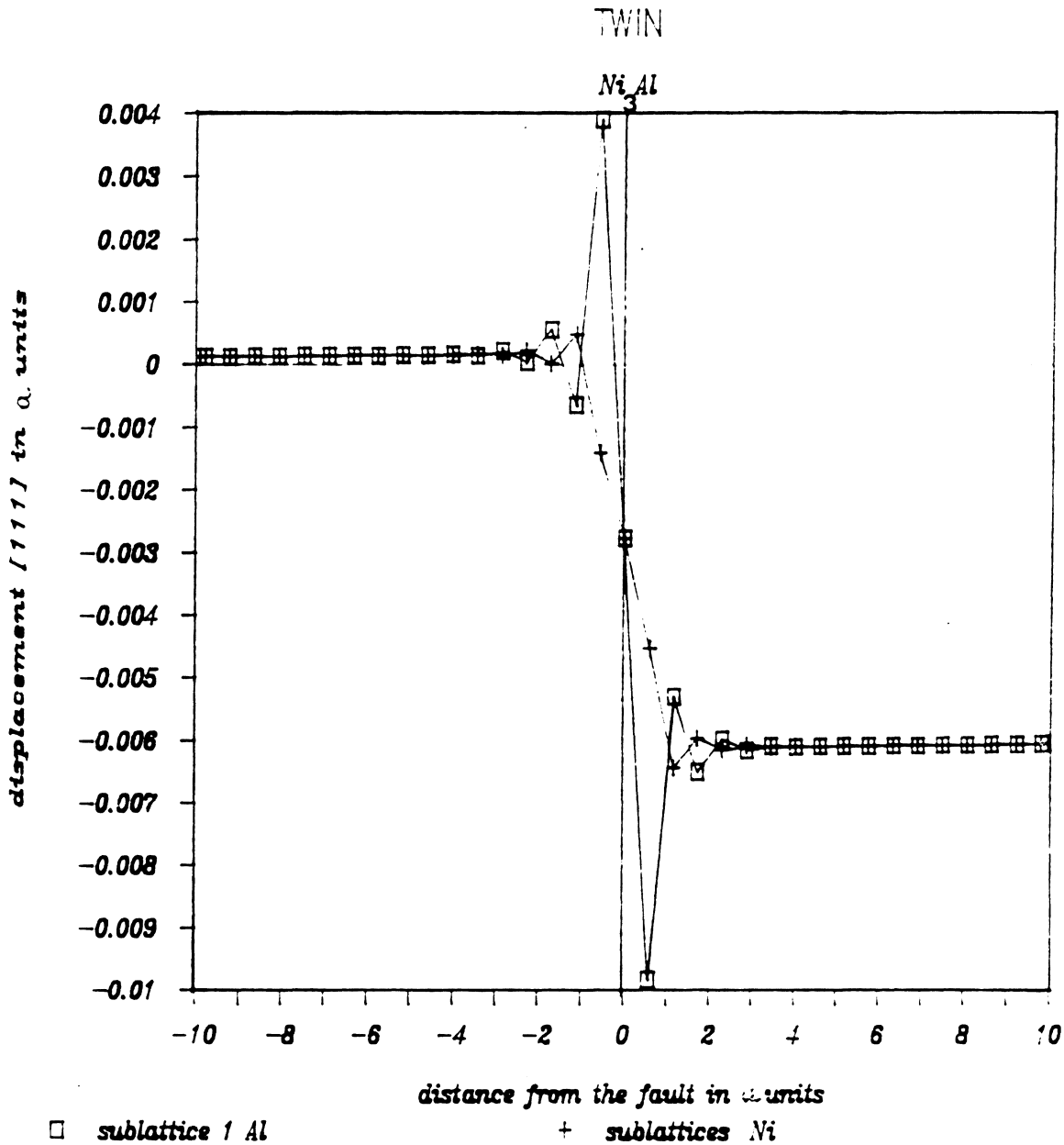

Figure 9. [111] Displacements of Atoms In Ni_3Al Away From (111) Twin

atoms about the twin boundary. However, the symmetry is not too obvious from the figure as as the rigid body displacement perpendicular to the boundary are explicitly included in the plot.

Two separate oscillation modes could be identified from the plots for Ni_3Al. In an attempt to separate these oscillation modes, the principle discussed in section 2.1.3. was used. Figure (10). represents the acoustic oscillation mode for Ni_3Al, this mode can be thought of as the displacements undergone by the center of mass of the motif. It is interesting to note that the acoustic oscillation of Ni_3Al has the same symmetry as the oscillations in Al or Ni. Similar displacements undergone by the atoms in the directions parallel to the boundary (that is the x and y directions) are shown in Figures (11 and 12). The oscillation observed in these directions are anti-symmetric and only the Nickel atoms are displaced.

Figure (13) shows the movement of the atoms in the (111) planes adjacent to the twin plane, and the arrows in the figure represent exactly the direction of motion of the atoms caused by the creation of the twin. The magnitude of the displacement is one hundredth of the length of the arrow.

6.2 Stacking Fault

The energy of the fault obtained is reasonably close to the previously reported results [21] of Chen and Vorter, while the latter workers used the same potentials, a different relaxation procedure was employed. The rigid body translation required to obtain the minimum energy configuration in the three metals and alloy are shown in Table 2. As in the twin the two halves of the crystal tend to push apart in the case of Al and Ni while in the Ni_3Al they tend to move closer.

Figure 14 shows the movement of atoms on the (111) planes adjacent to the super intrinsic stacking fault. The square atoms represent the first faulted plane and the triangles represent its unfaulted neighbor. The Al atoms are shown darkened. From this figure it can be seen that the Nickel atoms want to move towards the position that would have been occupied by the Aluminum atom if the crystal were unfaulted.

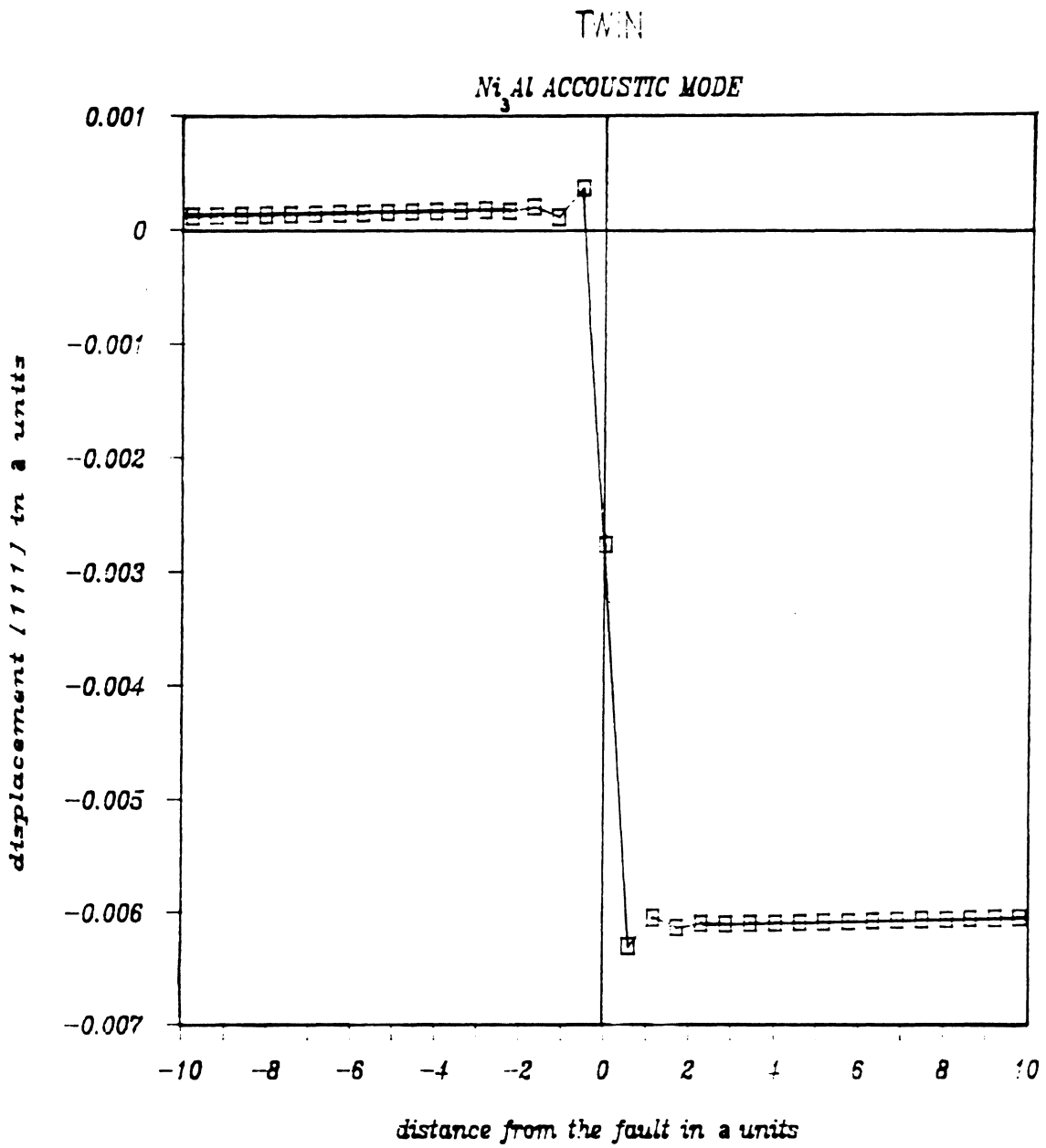

Figure 10. [111] Twin, Acoustic Oscillation mode in Ni_3Al

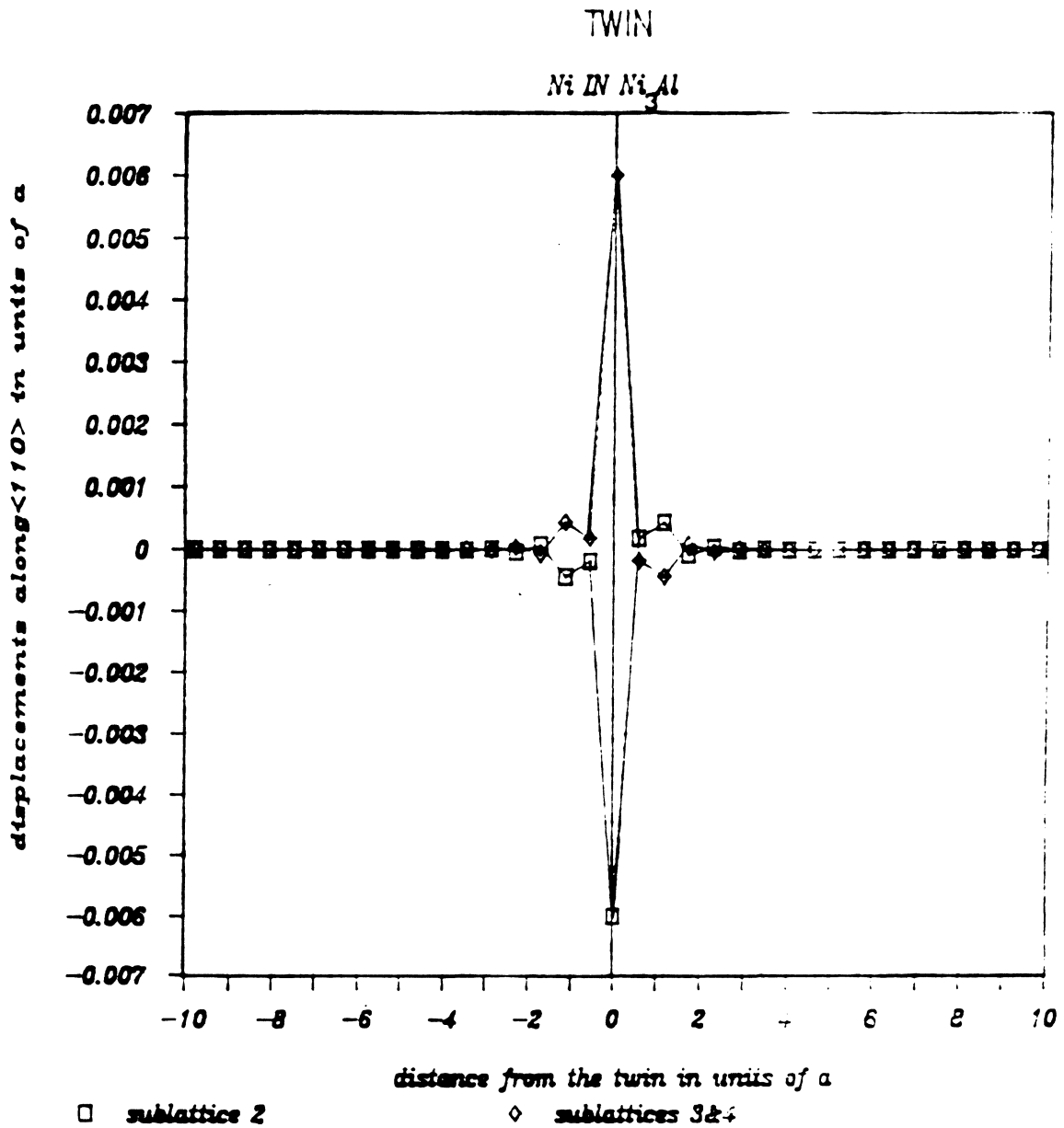

Figure 11. [1-10] Displacements of Atoms in Ni_3Al of (111) Twin

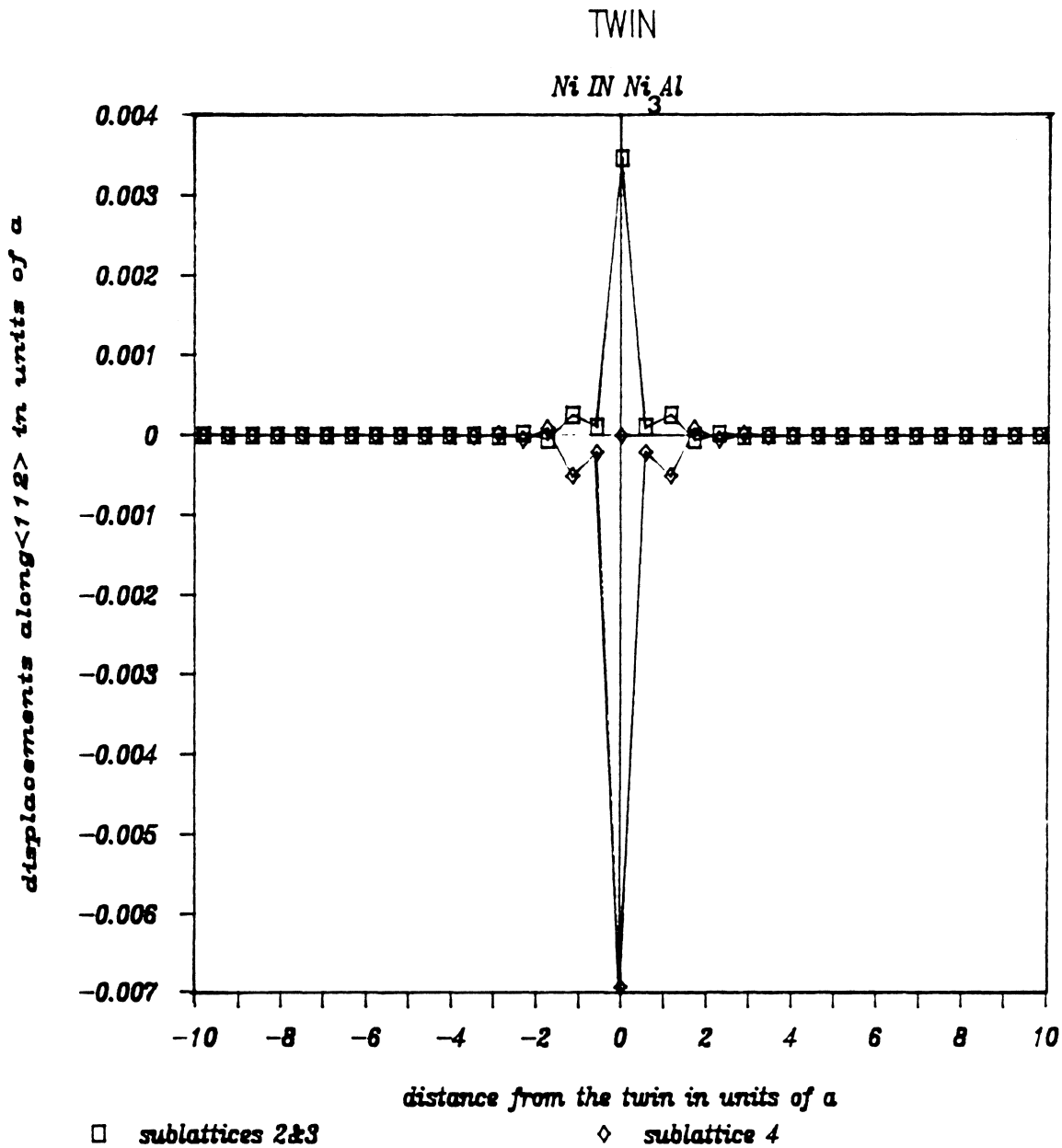

Figure 12. [11-2] Displacements of Atoms in Ni_3Al of (111) Twin

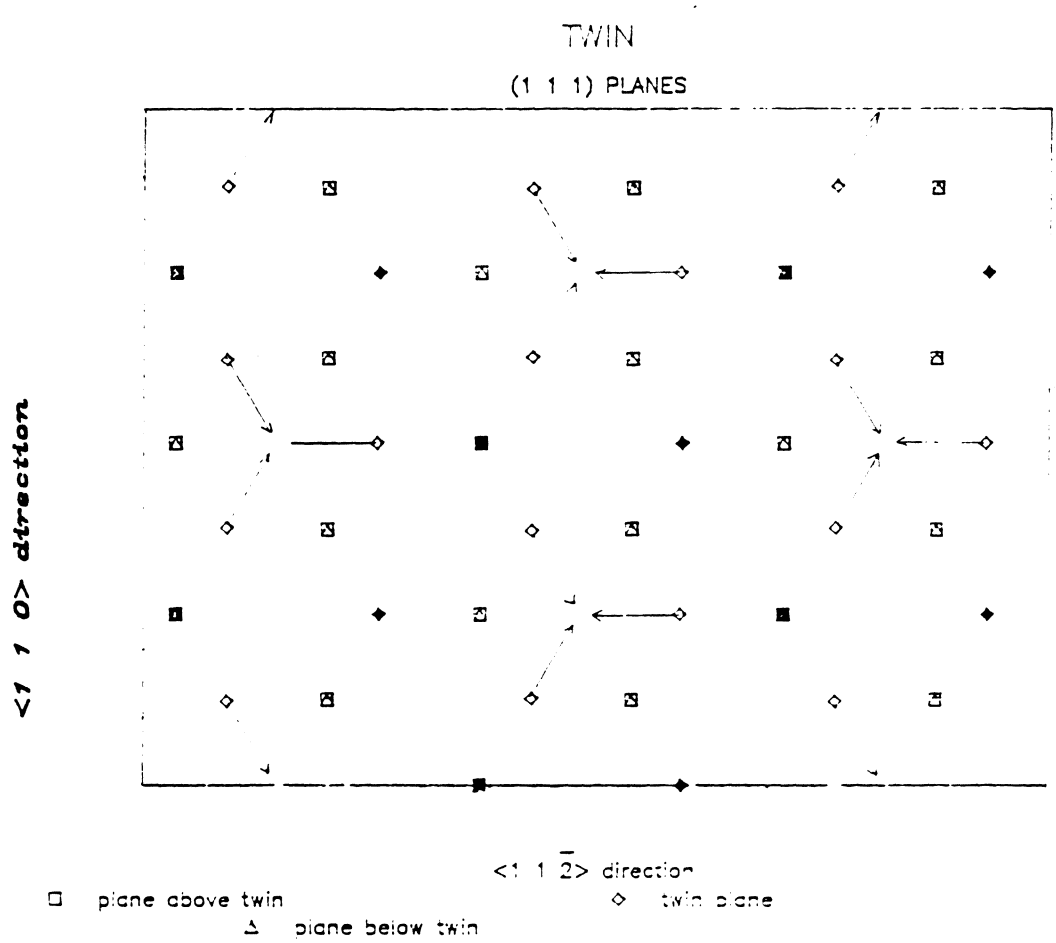

Figure 13. Displacements of Atoms in Ni_3Al of Twin on (111) Planes.

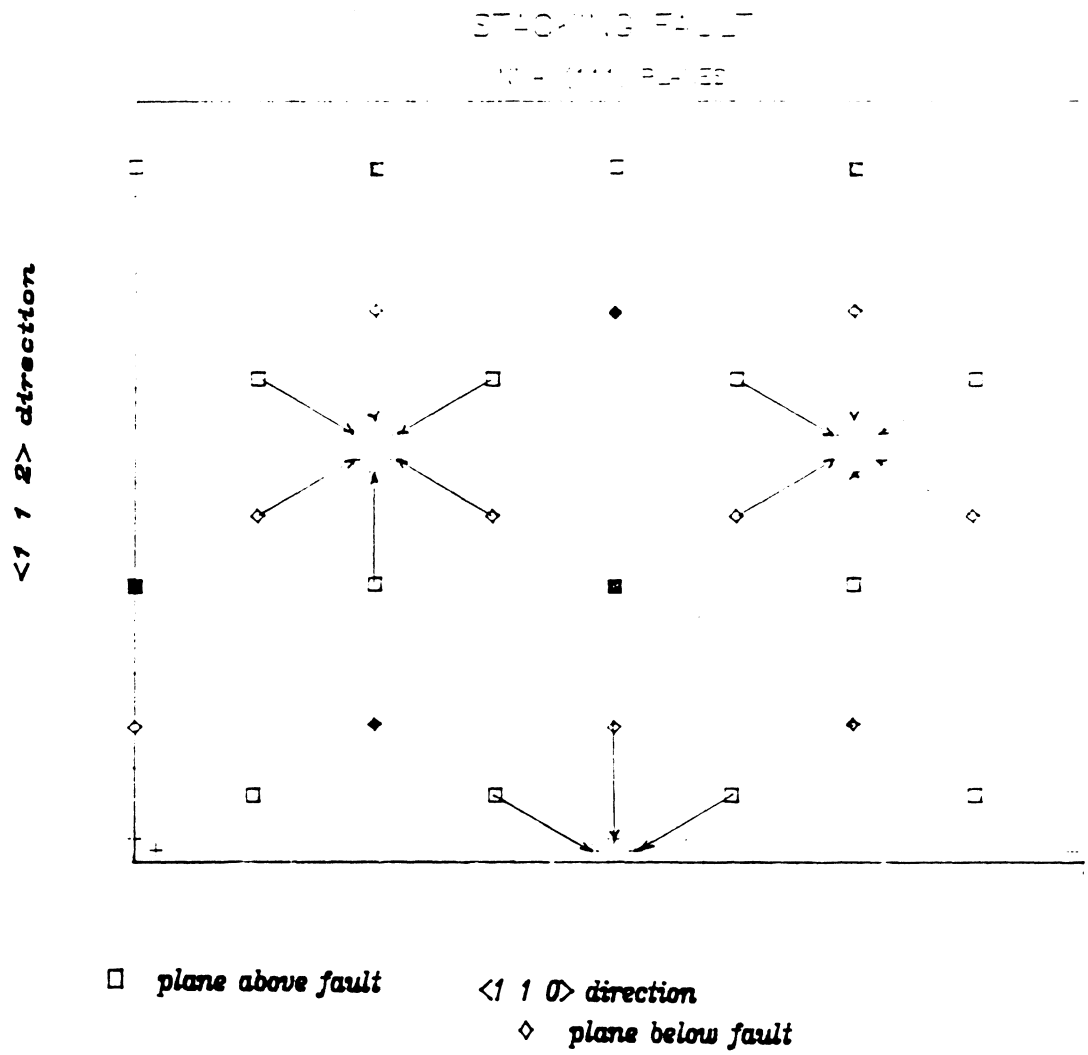

Figure 14. Displacements of Atoms in Ni_3Al of Stacking Fault (111) planes

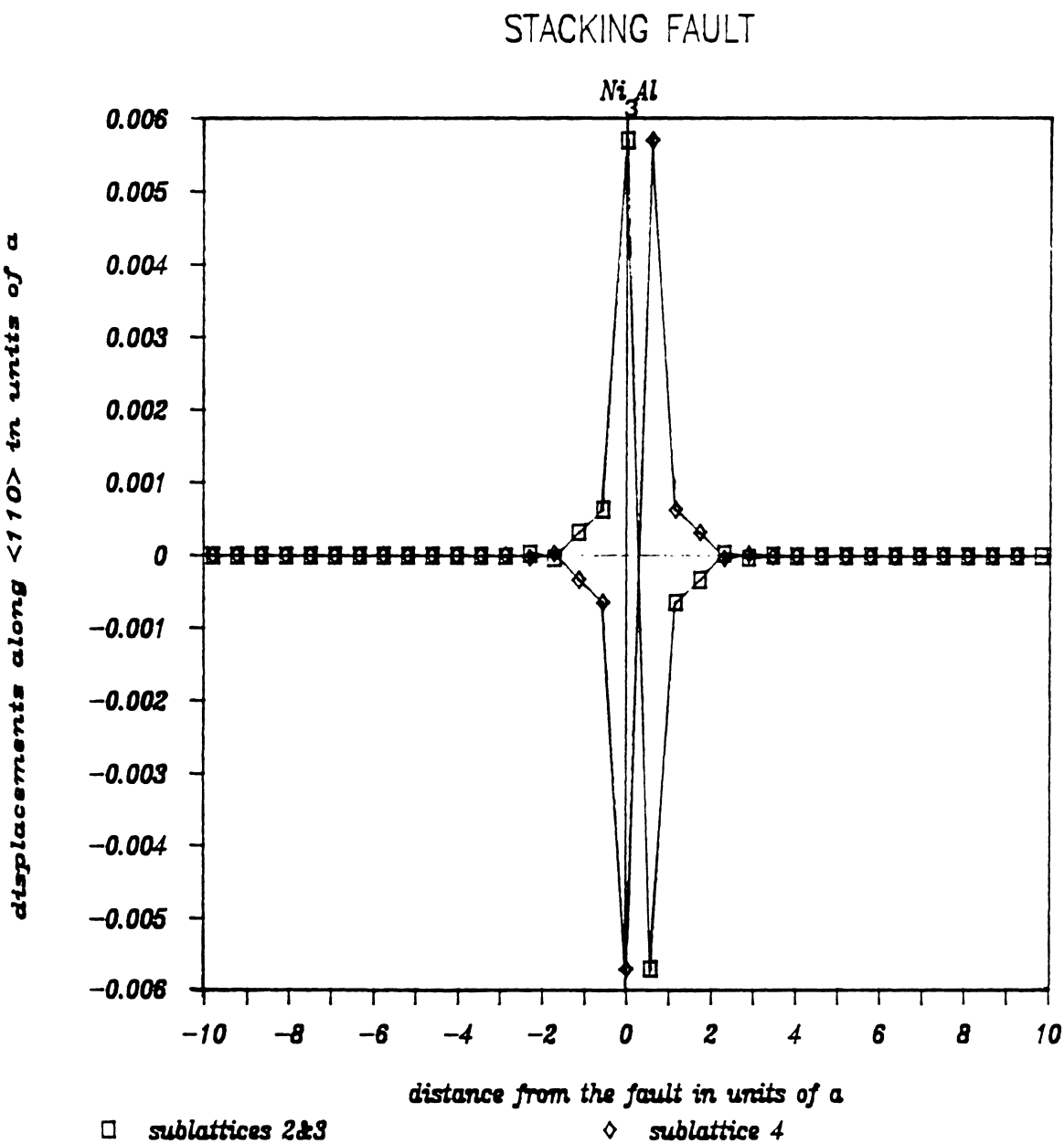

Figure 15. [1-10] Displacements of Atoms in Ni_3Al of Stacking Fault

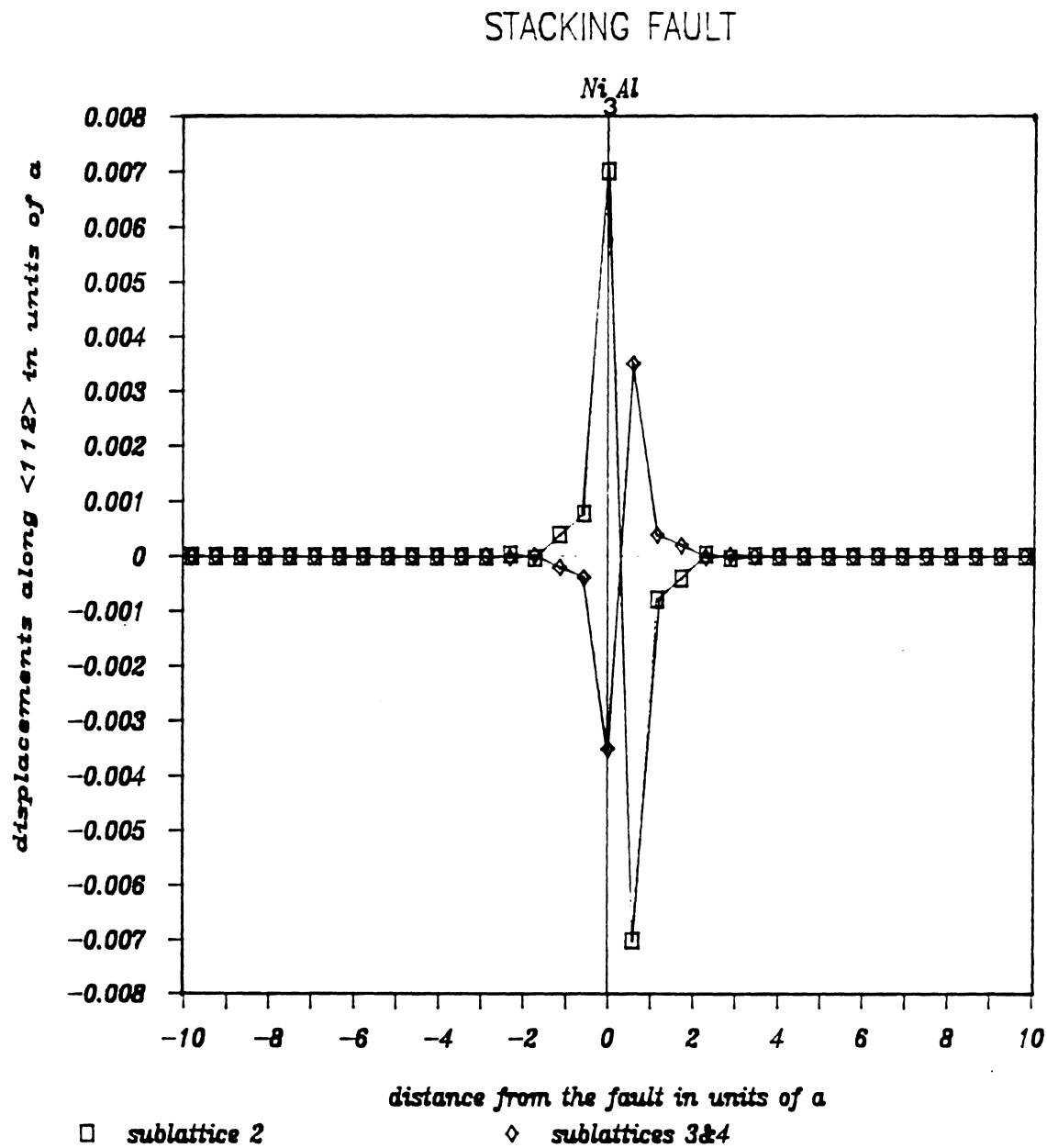

Figure 16. [11-2] Displacements of Atoms in Ni_3Al of Stacking Fault

Figure (15 and 16) show the displacement of atoms along the x and y directions and it is clear from these figures, and Figure (14), that the Aluminum atoms do not move in directions parallel to the defect plane. The parallel displacements of the Ni atoms are anti-symmetric about the fault (that implies that the vertical axis in figure (15,16) is a line of symmetry).

6.3 Anti-Phase Boundary

The anti-phase boundary (A. P. B.) has a similar defect structure as a superintrinsic stacking fault, and A.P.B is bound by a pair of $a/3 < 211 >$, superpartial dislocations [42]. However, the energy of an A.P.B is considerably more than that of a stacking fault. This is quite natural as the formation of an A.P.B. forces a Nickel atom to an Al atom position. The A.P.B. also creates a Al- Al bond and its bond length is about 27% more than the equilibrium Al-Al separation. Unlike the previous results, the Al atoms close to the A.P.B. also undergo a displacement in the direction parallel to the boundary. The relative displacements undergone by the Nickel and Al atoms can be seen in the Figure (17). The movement of atoms on a {110} plane on the domains on either side of the A.P.B. are also shown in this figure. Quite unlike the other planar defects the anti-phase boundary does not require a rigid body displacement in the direction perpendicular to the anti-phase plane. Since the Aluminum atoms also move in the [211], (Figure(18)), an acoustic mode of oscillation is also observed in this direction as can be seen from the Figure (19). Figure (20). shows only the antisymmetruc optical oscillations in the [110] direction.

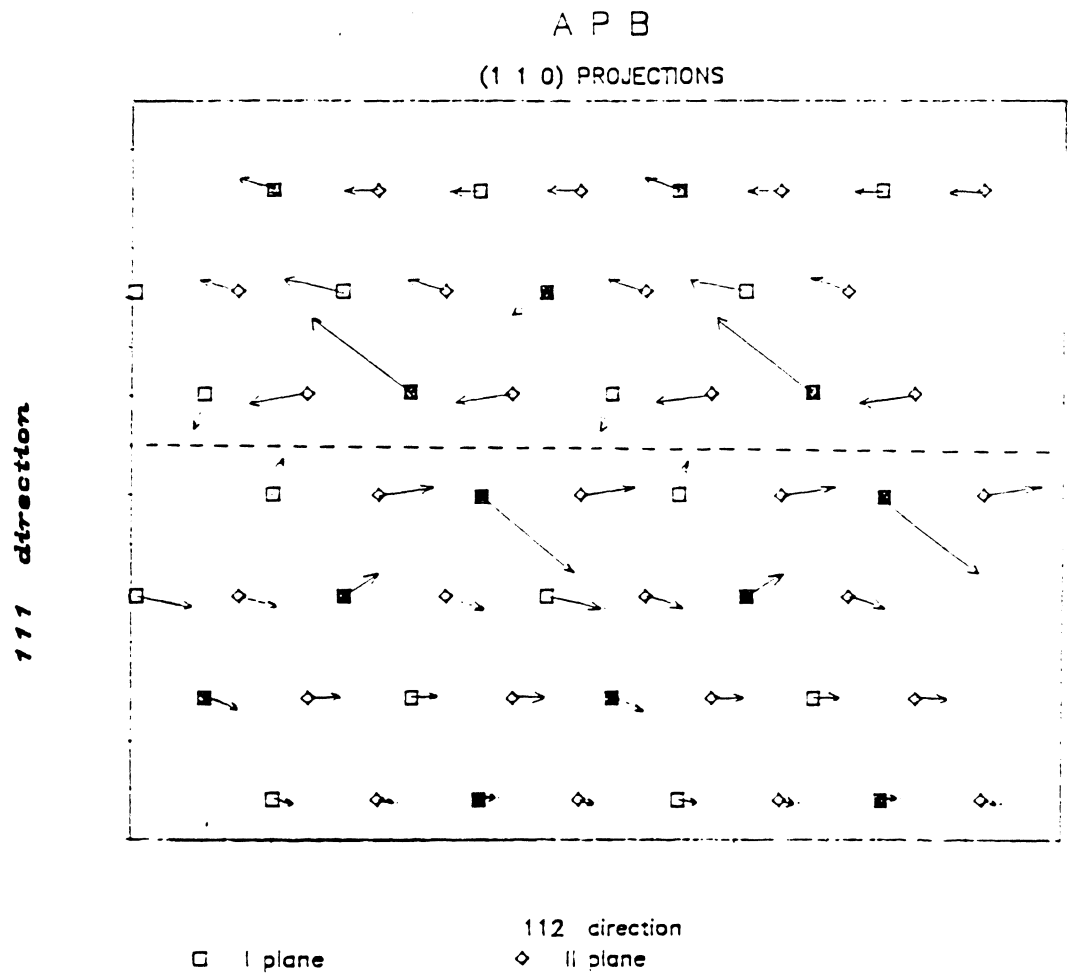

Figure 17. Displacements of Atoms in Ni_3Al of Anti-Phase Boundary on (1-10) Planes

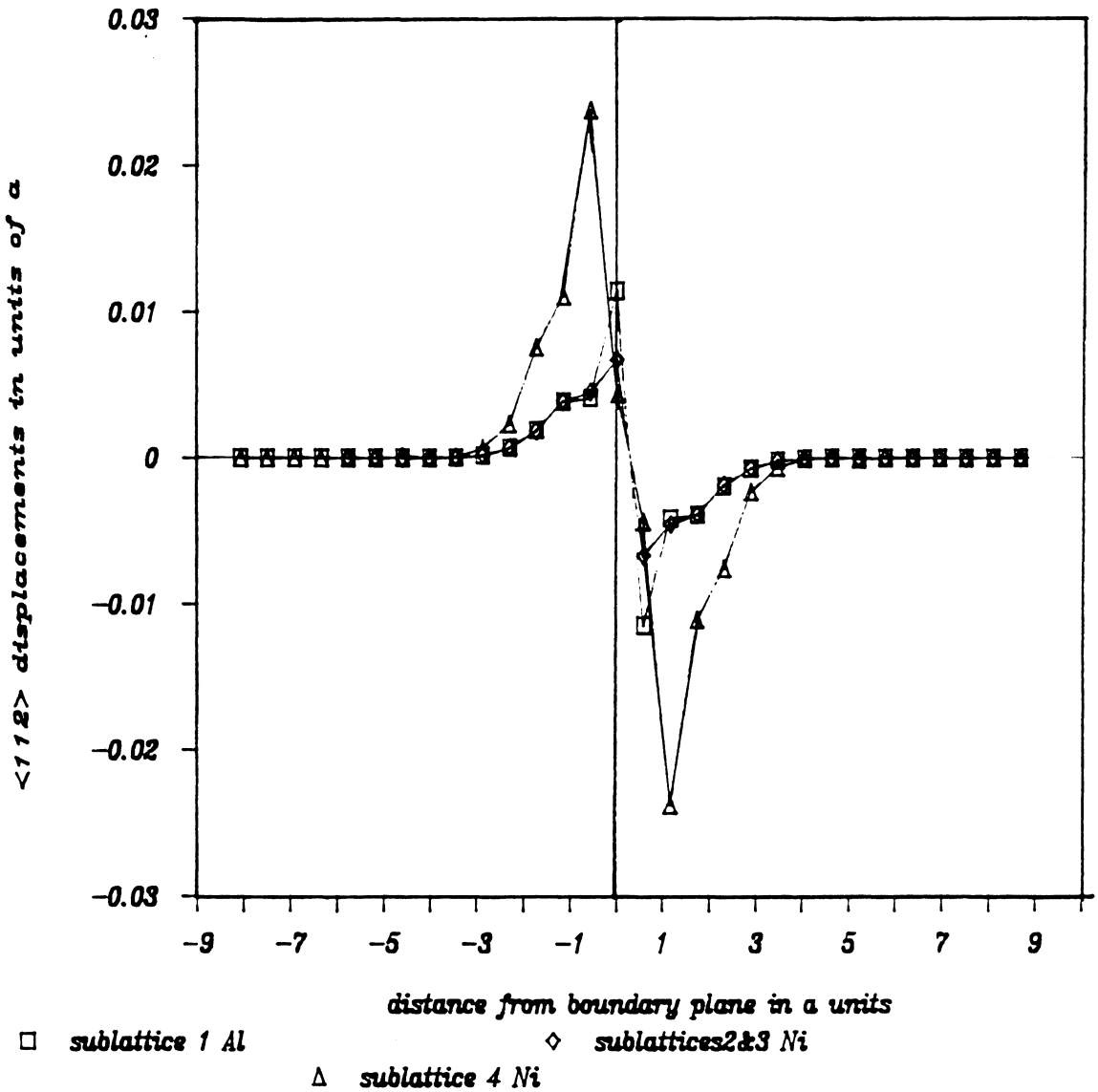

Figure 18. [11-2] Displacements of Atoms in Ni_3Al of Anti-Phase Boundary

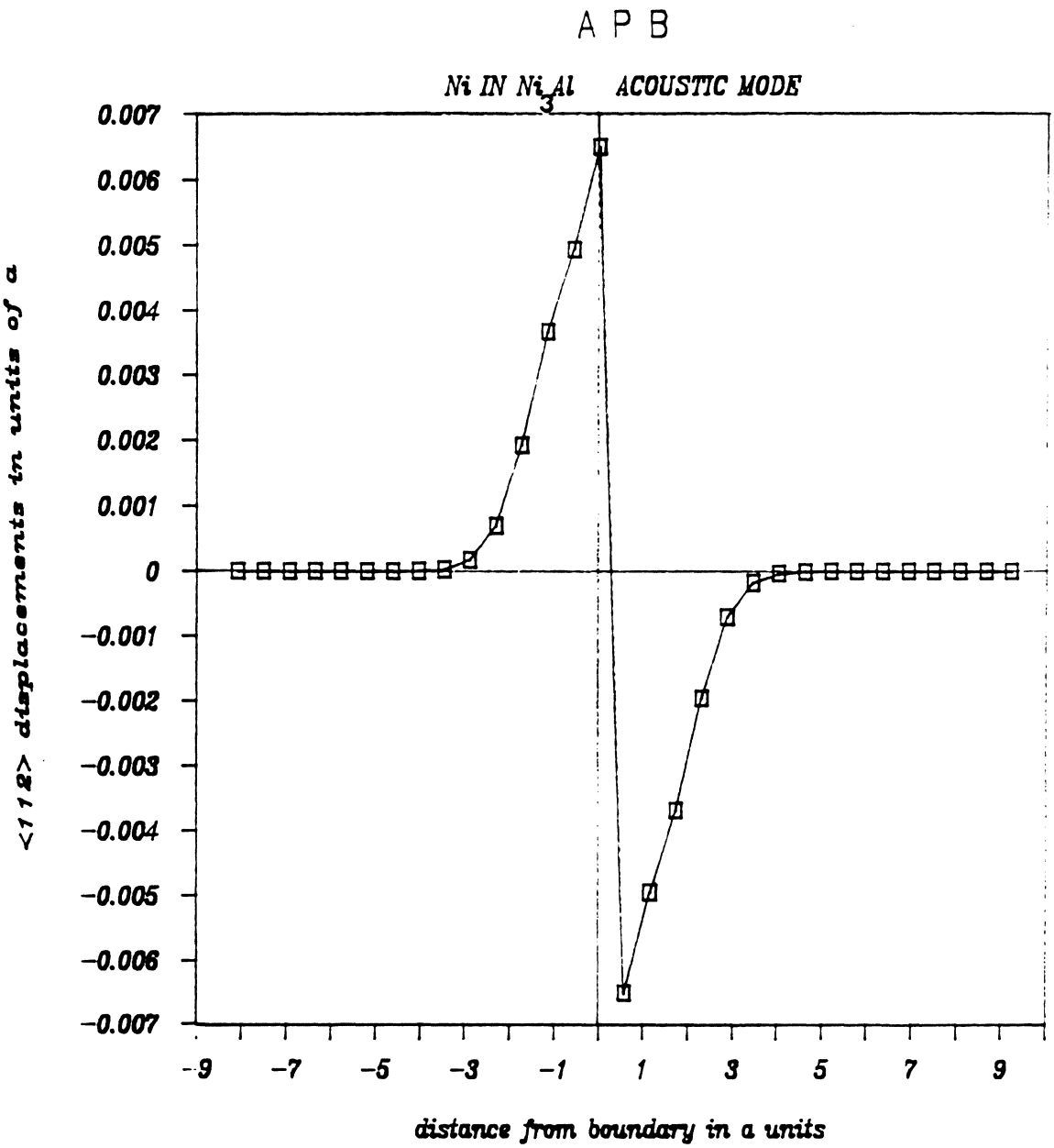

Figure 19. [11-2] Displacements Acoustic Mode in Ni_3Al of Anti-Phase Boundary

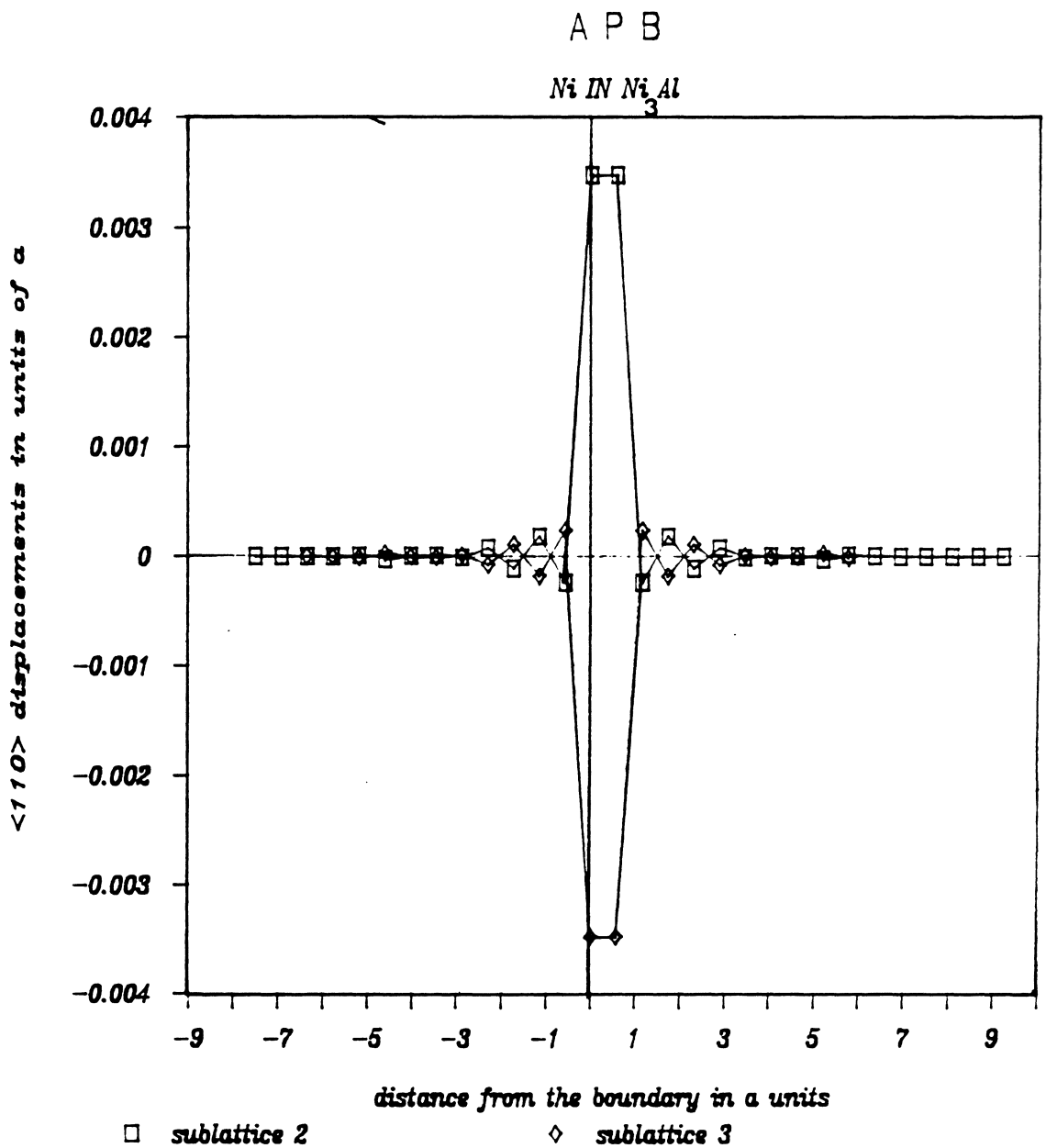

Figure 20. [1-10] Displacements Optical Mode in Ni_3Al of Anti-Phase Boundary

6.4 *Surfaces*

Computer simulation studies of surfaces were first reported by Chen et al [40]. They concluded from their studies that surface relaxation in Ni_3Al consists of an oscillatory relaxation that decays exponentially with distance into the bulk and furthermore a surface rippling was found to superimposed on this. The so called 'rippling' as reported by these authors, is the equivalent of the optical mode of oscillations discussed here.

The results obtained from surface studies on the (111), (100) and (210) planes are reported here and these results compare reasonably well with the previously reported results. The energy of the surface apparently seem to depend upon the density of atoms in the in the terminating plane. Hence the energy of the (100) is higher than that for the other two surfaces.

From Figure (3). it can be seen that the {100} planes can have two different possible compositions, 100 % Ni or 50 % Ni, 50 % Al. Consequently the properties of the {100} plane are expected to depend on the composition of the plane under consideration. For this reason calculations were done on both possible terminations. The same is also true for the {210} planes.

The oscillatory relaxations are obvious only in the less symmetric (210) surface. Figure (21) shows the variation of the interplanar spacing with the depth of the plane from the surface for Ni, Al and Ni_3Al cases. The change in the interplanar spacing is defined by the equation (6.1)

$$\Delta d_{n,\,n+1} = d_{n+1} - d_n \tag{6.1}$$

The oscillations are quite similar for Al and Ni, though they are of different magnitude. The oscillations of the Ni_3Al are shown for both possible terminations. In each termination the behavior of Al and Ni sublattice 3 (see figure (3)) is different from those of the Ni sublattices 2 and 4. The dotted lines in figure (21) indicate the two different behaviors and the solid line represents the average lattice separation. The oscillations of Ni_3Al are very close to those of its pure components. The exponential decay of the oscillations observed by Chen and co-workers, is apparent from this figure also.

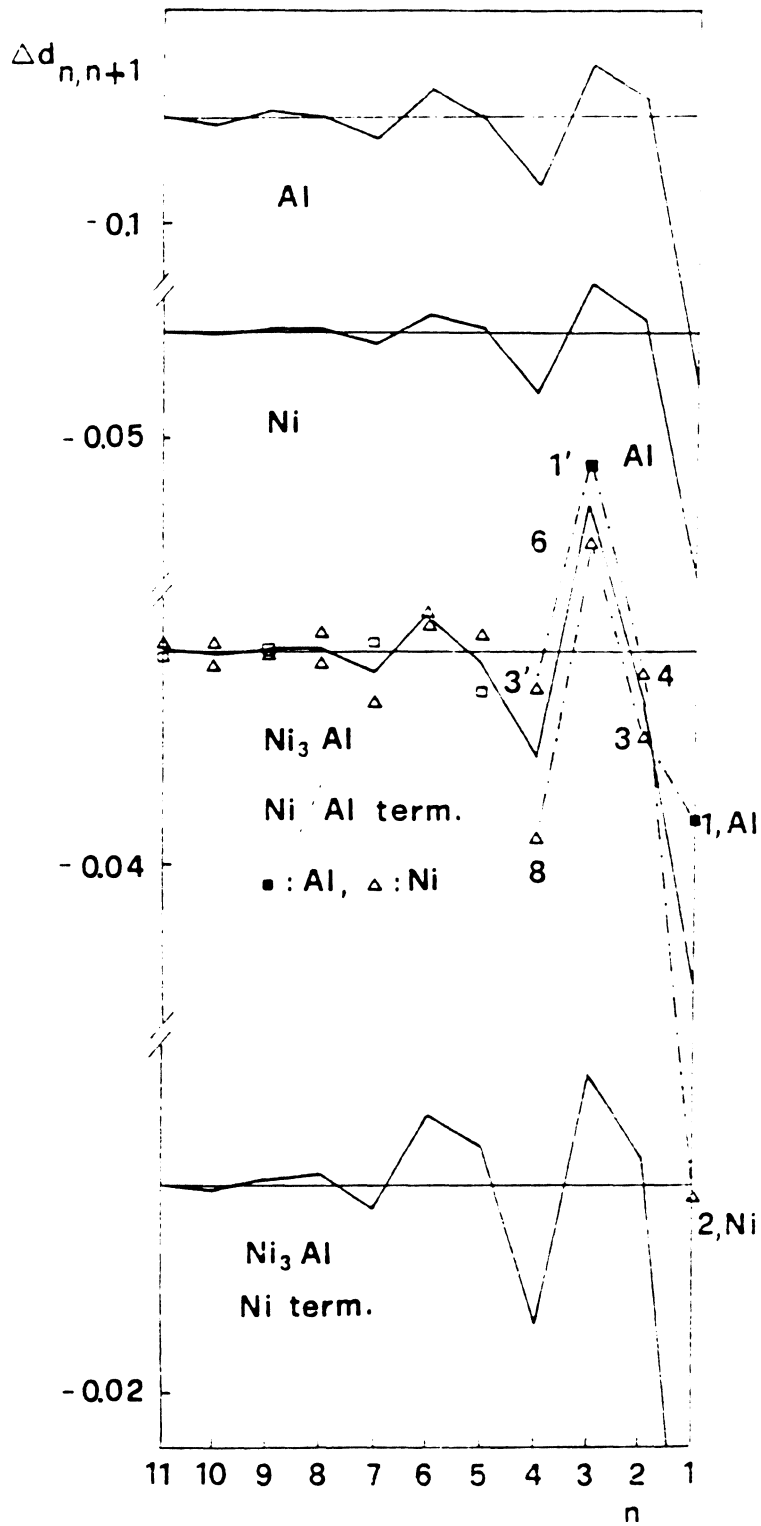

Figure 21. Variation of Interplanar Spacing in (210) surface of Ni, Al and Ni_3Al

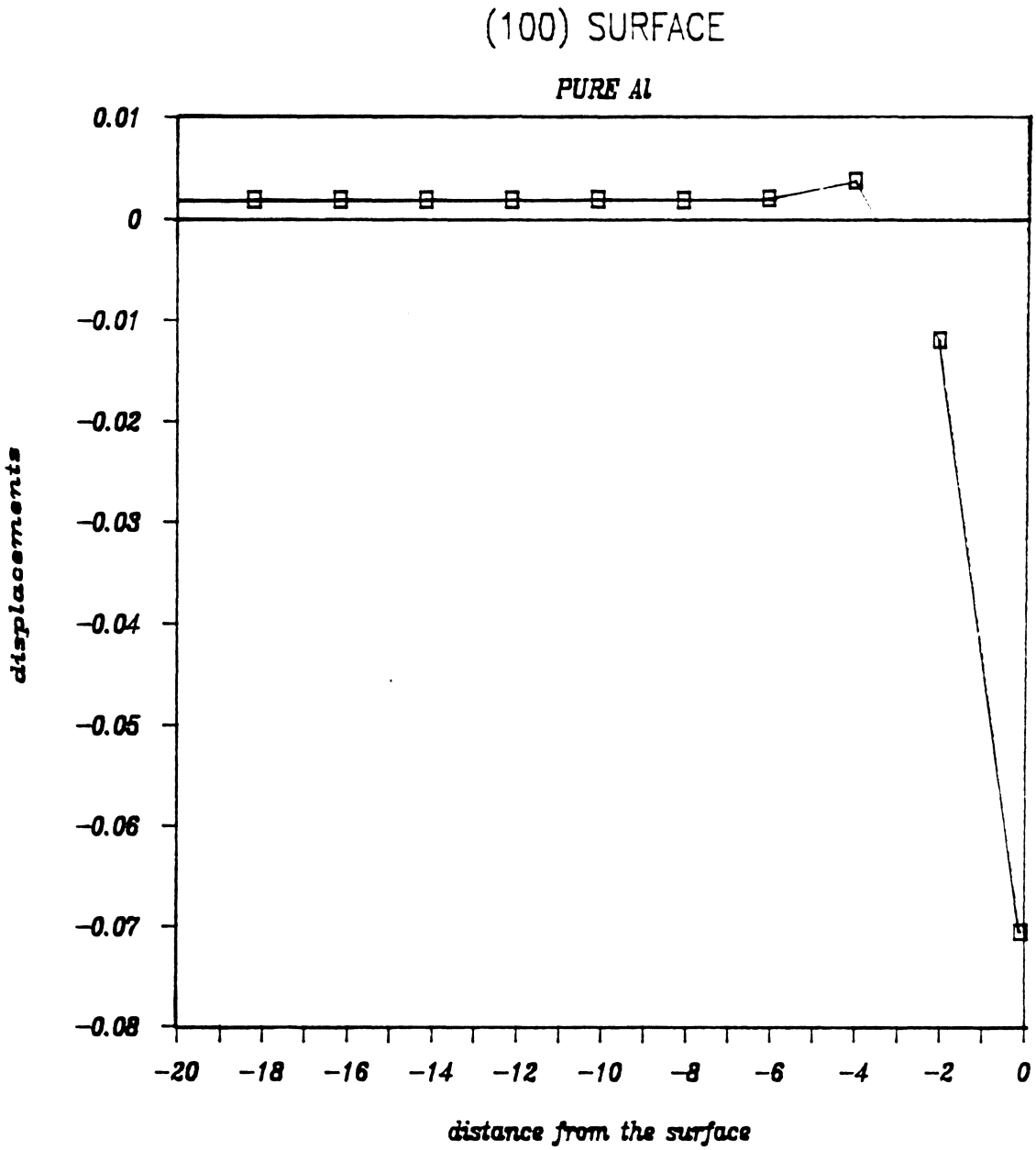

Figure 22. [100] Displacements of Atoms In Aluminum from (100) Surface

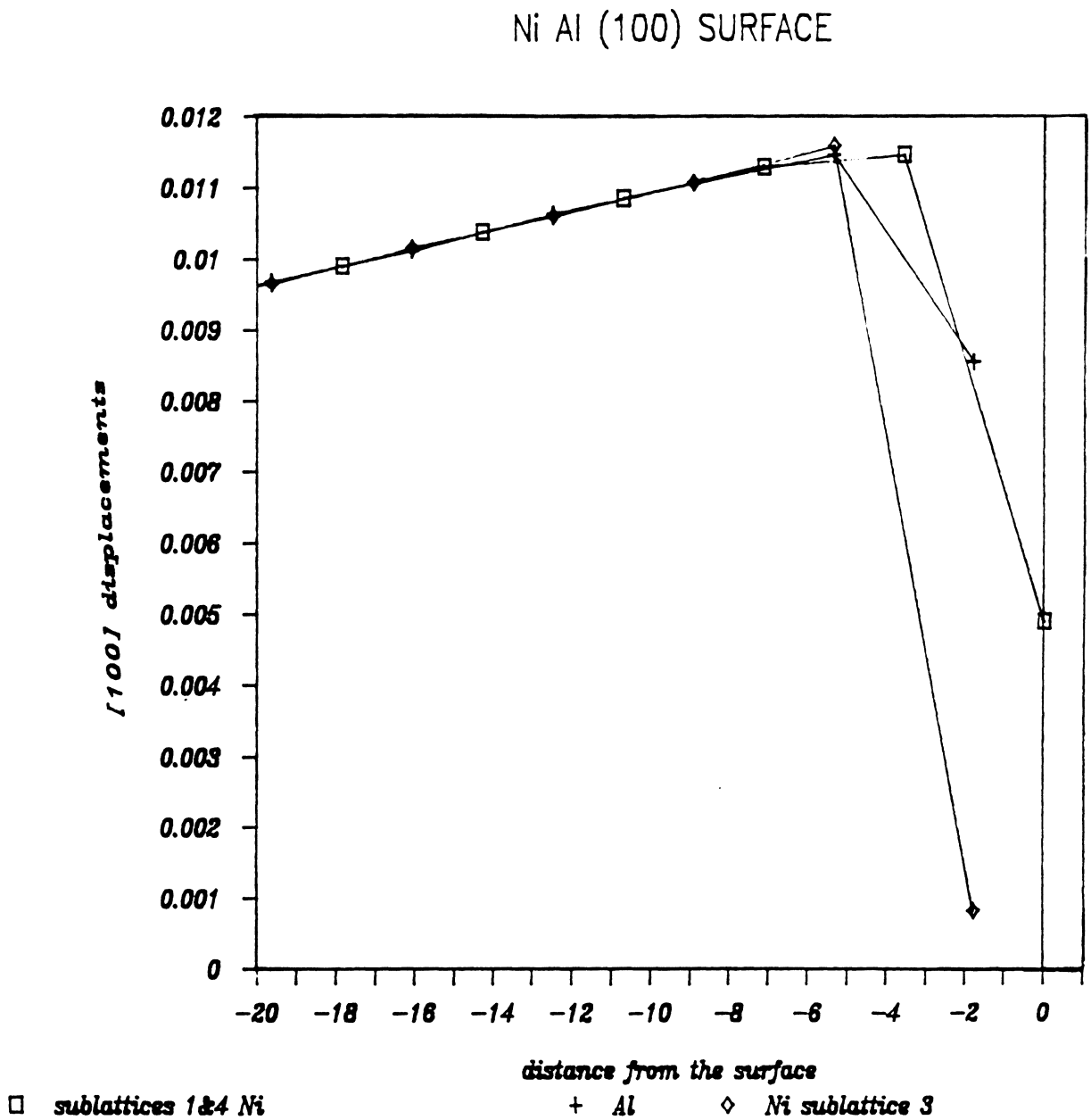

Figure 23. [100] Displacements of Atoms In Ni_3Al from (100) Surface

Figure (22, 23) show the displacement of atoms perpendicular to the (100) surface termination for Aluminum and Ni_3Al respectively. A very similar behavior was observed for Nickel also. There are no oscillations seen in the relaxation of this surface, and the magnitude of distortion induced is the maximum observed for any defect in this study. Even when, over 100 planes for Δz were used, (Δz is the number of planes perpendicular to the surface), the displacements did not appear to die out. Credibility of this calculation for the (100) surface is in fact questionable as the distortions are restricted by the atoms in Region II. (see figure (5).)

Figure (24) shows the movement of the atoms on the surface (111) plane and the next two planes immediately beneath it. The Aluminum atoms do not move in the direction parallel to the surface and the movement of the Nickel atoms is such that the center of mass of the motif is not disturbed.

6.5 Structure of $\Sigma = 5$ Boundary

The symmetric tilt boundary $\Sigma = 5$ (210) [100] was studied in detail. The structure of this boundary and the nature of its interaction with the vacancy are reported here. As stated before, in Ni_3Al two different {210} planes are possible. They can either have 100% Ni atoms or 50 %Al and 50 % Ni atoms. Therefore, three different (210) boundaries are possible, following the nomenclature used by Chen et al [24], we can identify them as 50/50, 50/100, 100/100 boundaries. A 50/50 boundary would refer to the boundary whose touching planes from either crystal have a composition of 50 % Ni and 50 % Al, similarly a 50/100 boundary implies that one of the boundary planes contains all Nickel atoms while the other has equal amounts of Ni and Al atoms.

Figure (25). shows the structure of the $\Sigma = 5$ (210) [100] 50/50 boundary in the Ni_3Al. The square atoms shown in represent the Aluminum atom while the atoms depicted by a plus sign represent Nickel atoms. The (100) planes are differentiated by shading one of them. The structure of the boundary observed here differs mildly from the results reported by D. Farkas and

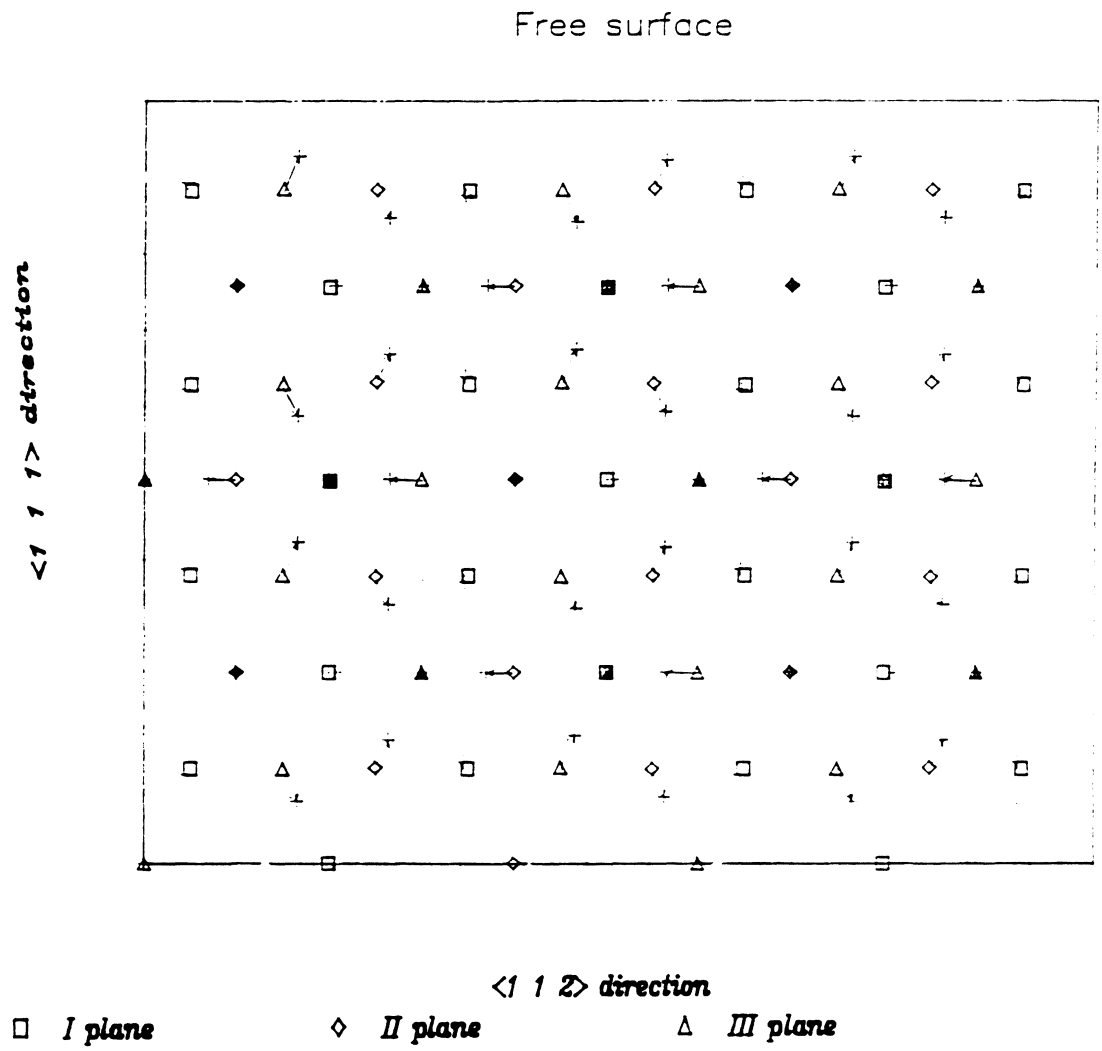

Figure 24. Displacements of Atoms in Ni_3Al of Surface (111) planes

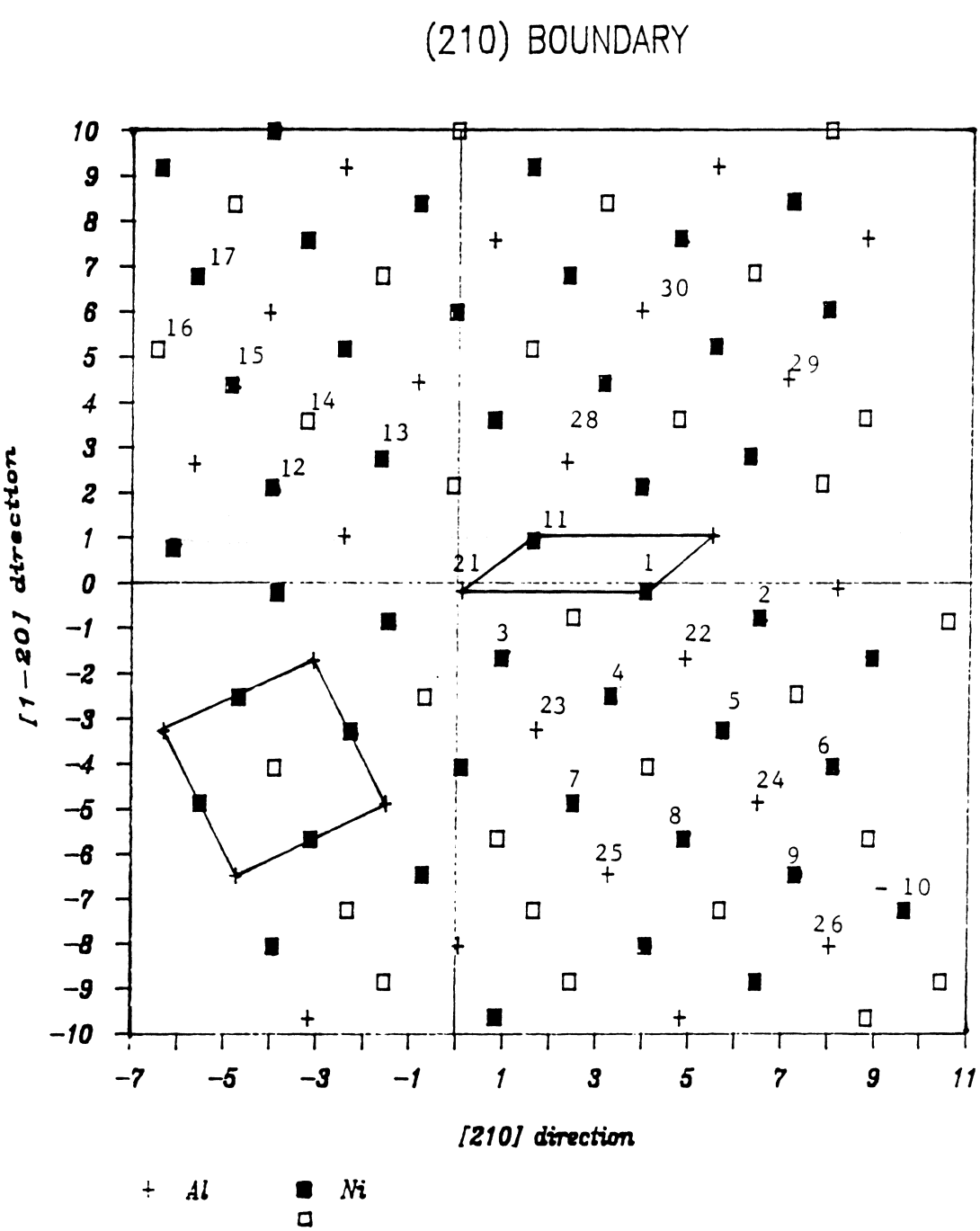

Figure 25. Structure of Σ = 5 (210) [100] 50/50 boundary
: repeating structural unit and the unit cell are deliniated

Rangarajan [41] which were based on their calculations using hard sphere geometric models. In contrast to their results the equilibrium boundary structure obtained here seem to require a rigid body shear between the two crystals. Apart from the rigid body translation given in the direction perpendicular to the boundary, the grain boundary requires a translation in the (1-20) direction parallel to the boundary. Figure (26) is a plot of the displacements undergone by the atoms as a function of their perpendicular distance from the boundary. As mentioned earlier (section 5.1.6), formation of a grain boundary absorbs certain atoms on the boundary plane. This causes a dissimilarity in the movement of the atoms, and therefore the plot appears unsymmetric. Even from this figure the oscillatory relaxation of the atoms can be seen.

6.6 Grain Boundary Interaction with the Vacancy

The formation energy of a vacancy is defined as the energy required to create a vacancy at any particular lattice site. The term Ni vacancy is used to identify a vacancy that is formed by removing a Nickel atom, similarly an Al vacancy is formed by the removal of an Aluminum atom. The energy required to create a vacancy in the lattice in the absence of any kind of defect is the vacancy formation energy or the formation energy of a vacancy in the bulk. The vacancies were created individually at positions close to the boundary and the variation of formation energy with their relative position from the boundary was studied.

Figure (27 and 28) show the variation of the formation energy of a vacancy (F. E. V.) with the distance from the boundary plane for Ni and Al vacancies respectively. The lowest energy of formation is seen close to the boundary and it increases asymptotically to the bulk value. This value of energy reaches the bulk value at a distance of approximately 5 Å from the boundary.

The vacancy formation energy also depends on the local atomic density and the type of neighbors around the vacancy. To facilitate the reader in identifying the exact location of the vacancy each point is represented numerically in Figure(26,27 and 28) and the coordinates of these

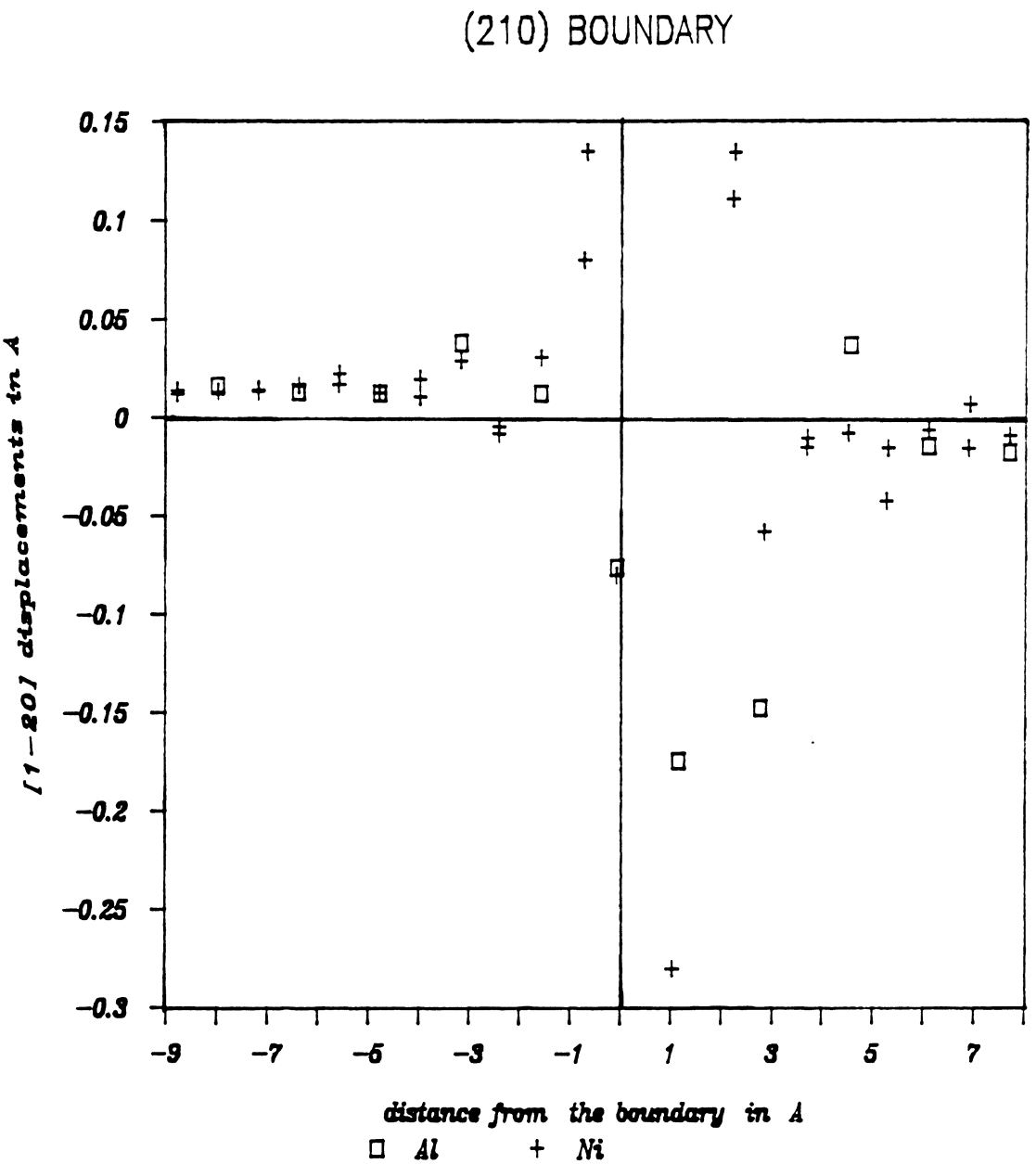

Figure 26. Atomic Displacements Perpendicular to the Grain Boundary

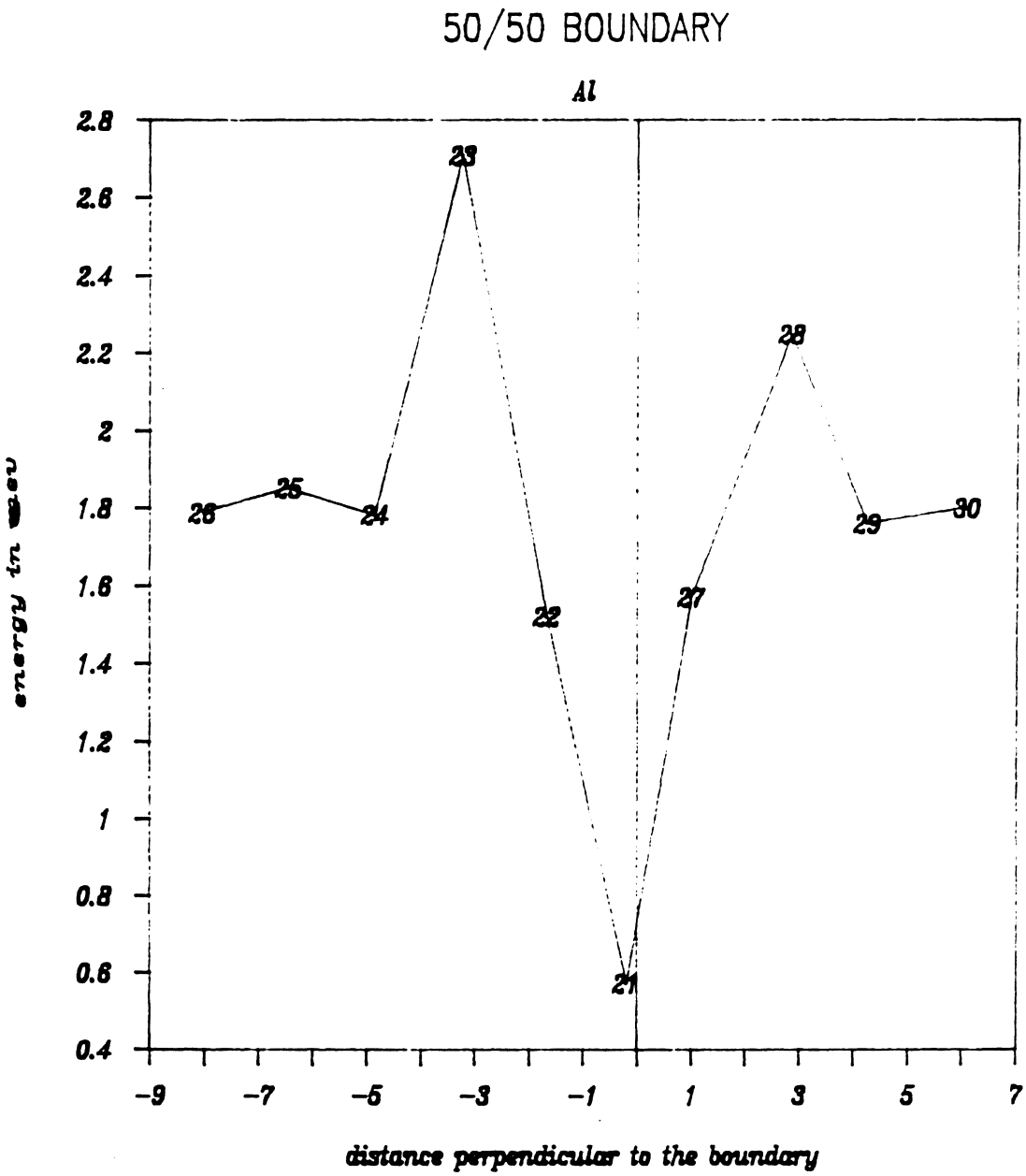

Figure 27. Formation Energy of a Al Vacancy
: all distance are in Å

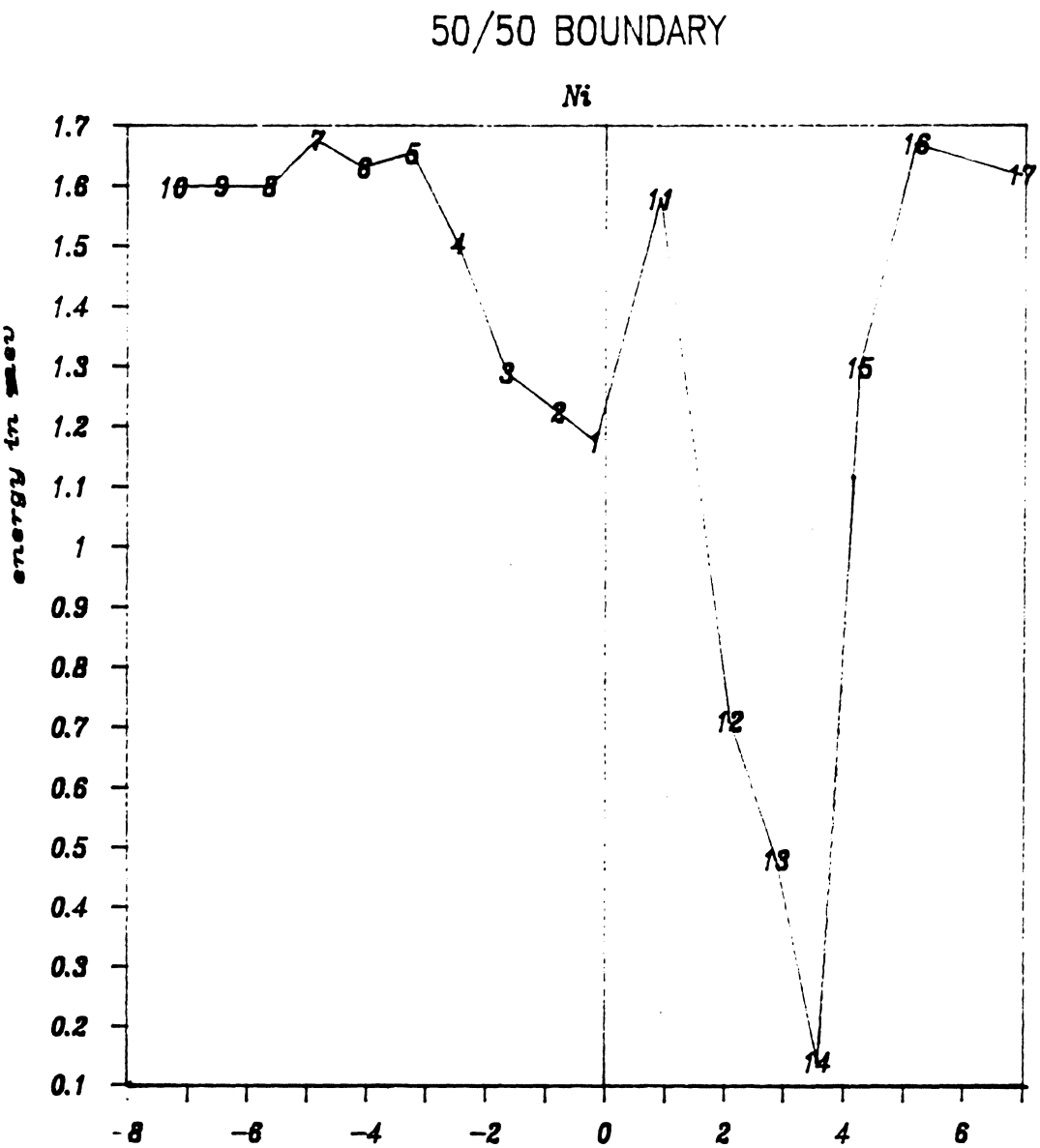

Figure 28. Formation Energy of a Ni Vacancy
: all distance are in Å

points are tabulated against the corresponding numerals in Tables 3 and 4. The location of the vacancy can also be matched to the lattice site by comparing the coordinates with Figure (25).

Table 3. Formation Energy of Aluminum vacancy

No.	Coordinates in Å		F.E.V in e.v
	[2-10]	[120]	
21	8	0.19	0.5747
22	11.2	1.67	1.5218
23	14.38	3.24	2.709
24	9.6	4.86	1.7845
25	12.78	6.44	1.853
26	7.99	8.04	1.787
28	2.5	-1	2.258
29	6.39	4.25	1.79
30	4.1	6.094	1.80
Bulk			1.82

Table 4. Formation Energy of Nickel Vacancy

No.	Coordinates in Å		F.E.V in e.v
	[2-10]	[120]	
1	12.06	-0.1751	1.579
2	9.62	-0.803	1.225
3	7.18	-1.675	1.29
4	12.8	-2.49	1.505
5	10.39	-3.25	1.655
6	11.98	-4.06	1.63
7	13.59	-4.85	1.677
8	11.59	-5.65	1.6
9	8.79	-6.45	1.6
10	10.39	-7.25	1.598
11	1.72	+ .901	1.579
12	-4.1	+ 2.08	0.71152
13	-1.62	+ 2.86	.48
14	-3.13	+ 3.56	.14
15	-5.00	+ 4.25	1.3
16	-6.58	+ 5.18	1.67
17	-5.89	+ 6.94	1.62
Bulk			1.62

7.0 Discussion

An analytical basis of the force discontinuity model for defect calculations has been established in chapter two. Kanzaki forces that are characteristic of a defect were used to obtain relation for the displacement fields. For point defects the Kanzaki forces have actually been estimated [7], and the Greens function techniques were used to calculate the distortions. However, these calculation are not well suited for near defect studies in strong defects. The author sees no reason why this technique cannot be used to treat the atoms that are in the fixed boundary (Region II in Figure (5).)

The results presented here and those published by Chen et al. [23,40 demonstrate that the potentials developed by the embedded atom method are capable of predicting the structure and properties of defects in Ni_3Al. Results obtained for defects like surface termination that causes a potential disturbance to the lattice are in good agreement with the experimental data [40]. Moreover Savino and Farkas [24], based on their comparative analysis of the simulation results from pair wise calculations and embedded atom method, have established the supremacy of the embedded atom method.

7.1 Oscillation Modes

The energy associated a with a defect lattice is more than that of a perfect lattice, this energy can be referred to as the formation energy of the defect. This energy is stored in the crystal by straining the lattice around the crystal. As a result the atoms on either side of the defect undergo a displacement from their perfect lattice position. The magnitude and direction of these displacements are found to depend on the position of the atom as well as the nature of the defect. When the displacements undergone by the atoms are plotted as a function of their corresponding distance from the boundary, as shown in Figures (17,18, 20, 21, 24) certain definite wave patterns were observed. For Ni_3Al two separate modes of vibrations have been identified. By analogy to the lattice vibration modes these two different modes of vibration are called the optical and acoustic modes. The analytical development to describe these algebraically and a brief description of their physical significance is given in section 2.1.3

The most interesting aspect of these lattice oscillations is that the optical modes are absent in pure components of the alloy namely, Aluminum and Nickel, as can be seen from Figures (17, 18, 20) One can unequivocally conclude, based on the above aspect, that the presence of different atoms in the Ni_3Al is the prime reason for the creation of the optical mode of oscillations.

It has been mentioned earlier that there are four different sublattices in the Ni_3Al and a motif consisting of three Nickel atoms and an Aluminum atom can be considered simply as a repeating lattice point. If a center of mass is assumed to exist at the weighted center of each motif, its movement under the influence of the Kanzaki force due to the defect can be called the acoustic mode of oscillation. The acoustic displacements were taken to be the weighted average of the displacements undergone by the four different atoms in each sublattice. The coordinates of the central sublattice point is assumed to be the position of the center of mass of the motif. The acoustic mode of oscillation was observed in the direction perpendicular to defect in all the defects that were studied here, while only the anti-phase boundary was found to have an acoustic relaxation mode in the direction parallel to the boundary, (see Figure (24). It is interesting to note here that the

acoustic oscillation is only seen in the direction along which the Aluminum atoms move. Therefore, it is reasonable to conclude that the direction of the center of mass of the motif is influenced more by the Al atoms. Hence it should be more reasonable to calculate the acoustic oscillations with different weight factors for Aluminum and Nickel. However because the physical basis for such a weight factor is difficult to establish in this study different weight factors were not used.

The movement of the different atoms in the sublattice of one motif is such that the center of mass of the motif is maintained. The size and charge variation between Al and Ni atoms could be the reason for these micro moments within the motif. In the unalloyed state Nickel and Aluminum do have many sublattices and each atom position is the lattice position by itself. Consequently the acoustic mode of oscillation of the alloy is similar to that for a pure metal. The different relaxation patterns of the atoms that belong to four different sublattice is the reason for the presence of the optical oscillations. Table 2 give a good idea on the nature of oscillations observed for various defects in different directions.

Figures (13 and 14). show the displacements of atoms on the defected (111) plane for a twin and super intrinsic stacking fault respectively. The fact that Aluminum atoms do not move in $\vec{x}$ and $\vec{y}$ directions suggests that the defect does not change the surroundings of the Aluminum atoms. The movement of the Nickel atoms is very interesting and is similar in both defects. Three Nickel atoms which can be assumed to belong to the same motif, displace such that the force polygon drawn from their displacement vectors would yield a zero net force. This means that the center of mass of the motif is not displaced by the movement of atoms in a direction parallel to the defect.

Surface termination causes a potential disturbance in the lattice, and hence the defect energy of a surface is some three orders of magnitude higher than the relatively weaker defects, such as stacking faults and twins. To store such large energies strain fields of larger magnitude are created and these extend very deep into the crystal. These strains create an observable change in the inter-planar spacing of the planes close to the surface. The local density at the lattice sites on the surface is dramatically lowered due to the absence of half of the neighboring atoms. Therefore, in the process of relaxation the surface plane move closer to the planes beneath it. Consequently, the

atomic density about the plane next to the surface is increased. This causes the next two planes underneath the the original surface plane to move away from each other. This sequence continues with a decreasing magnitude as one goes further beneath the surface thereby creating a oscillatory variation in the inter-planar spacing. The micro-moments created by the relocation of the atoms within a motif are of lesser magnitude than the acoustic oscillations and hence the optical modes are not obvious in Figure (21).

The change in the atomic density on the surface is even severe if the density of atoms in the terminating plane is low itself. For this reason, and since the inter-planar separation is a maximum for the (100) plane, huge strain fields are created and no oscillations are observed for the (100) surface termination.

The energy of an A.P.B. is an order of magnitude grater than that for a twin or stacking fault. As stated earlier, the generation of an A.P.B. causes a change in the type of neighbors that are present next to atoms forming the A.P.B. In the process of reaccommodation new bonds of different lengths are formed. A large fraction of the energy of an A.P.B. can be expected to be spent in holding Al - Al neighbors at a distance that is 27% more than their equilibrium bond length. The Coincidence Site Lattice model of a grain boundary identifies the boundaries by a "Structural Unit" that is found in certain favored boundaries. Similar repeating structural units can be identified, from Figure (17) in an A.P.B. also.

Grain Boundary

The formation of a grain boundary like any other defect creates a strain field around it. A study of atomic displacements as a function of their position relative to the boundary, as shown in Figure(26), does not reveal much information since the atomic displacements also depends on other factors. Atoms close to sites that are absorbed by the boundary undergo a larger displacement compared to the atoms that are further from those sites, but at equal distance from the boundary.

A periodic array of a [2-10] and a [120] primary dislocation that define the boundary can be observed from Figure (25). The grain boundary structure correlates reasonably well with the presently accepted structure. The repeating structural unit called the 'primitive cell' of the boundary can be identified on the boundary plane. As can be seen from the same figure the atomic density on the boundary plane is relatively low. A migrating species can therefore tunnel through the vacant areas in the boundary with relative ease. As a consequence the grain boundary can be thought of as a high diffusivity path in the crystal.

7.2 Grain Boundary Interaction with the Vacancy

The formation energy of a vacancy seems to depend on many different factors, therefore it becomes difficult to to rationalize the behavior. Very obvious influences are from

- the perpendicular distance between the vacancy and the boundary.
- the local atomic density in the vicinity of the vacancy.
- composition of the {001} plane on which the vacancy is formed.

When the formation energy of a vacancy and the magnitude of displacements undergone by the boundary are studied as a function of their distance perpendicular to the boundary, two exactly opposite functional dependencies can be observed (compare Figure (26) and (27,28)). The formation of a vacancy causes a strain field independent of other defects in the material. Using the continuum approach, the stress generated by a vacancy can be thought of as being tensile while the ones due to the grain boundary are essentially compressive (it should be mentioned here that, there are certain specific sites close to boundary where the stresses may be tensile in nature). Therefore the energy of formation of a vacancy is lower at the boundary than in the bulk.

The formation energy of a vacancy reaches the bulk value at a distance of approximately 5 Å from the boundary. Since the presence of the boundary exerts little influence beyond a distance of 5 Å, it can be concluded that the $\Sigma = 5$ grain boundary thickness is approximately 10 Å in Ni_3Al.

The lowest formation energy of a Nickel vacancy is found at a site that does not lie in the boundary plane. However it is interesting to note that the formation energy is lowest at sites where crowding is maximum. Since the density of the atoms at the grain boundary is lower than its adjacent plane, the immediate neighbors to the grain boundary plane can therefore act as better sinks for vacancies. Since the displacements undergone by the atoms close to the boundary are of the order of a tenth of the lattice spacing it is difficult to distinctly define the boundary planes.

The vacancy that exists on a (001) plane of composition of 100% Nickel has different neighbors than that on a plane with 50% Nickel and 50% Aluminum. In Figure (28), the energy of formation of vacancies at sites 6 and 8 are relatively lower than the ones for sites 7 and 9. Hence we can conclude the Nickel atom neighbors are conducive to vacancy formation.

The difference in the formation energy of the vacancy in the bulk and at the grain boundary could give a good idea of the driving force required for a vacancy that is already present in the bulk to migrate to the grain boundary. From our results we can see that the energy gradient for Al vacancy is 1.2 ev as compared to 1.65 for Ni. It is interesting to note that though the formation energy of the vacancy for Al is more than Ni, this energy gradient extending from bulk to boundary is less than that of Ni therefore there is a grater probability that a Ni vacancy will migrate to the grain boundary than an Al vacancy.

Any defect that causes a radical change in the neighbors of any Aluminum atom causes the energy of the defect to be relatively higher than the ones that do not disturb the Aluminum atom. For example the anti phase boundary causes more distortion to the lattice than the Stacking fault, even though the mechanism involved in the generation of the two defects are very similar. And the 100/100 boundary where no Aluminum atoms are present in the boundary plane is of lower energy than the other two $\Sigma = 5$ (210) [100] boundaries [24].

8.0 Conclusions

1. While the analytical calculations can be used to estimate the displacements of atoms around planar defects, they cannot be used to study the atoms close to the defect.

2. Two distinct oscillation modes are observed in Ni_3Al. The symmetric acoustic oscillations arise as a consequence of a direct effect of the Kanzaki force of the defect being considered and the optical mode is created by the micro-moments caused by relaxation of atoms within a motif. By separating the forces into symmetric and anti-symmetric components, equations (2.20, 2.21) which describe these oscillations can be derived.

3. The lowest energy defect structures apparently require rigid body translations. The rigid body translations that are necessary and the energy of the defect being considered are tabulated in Table(3).

4. Simple repeating "structural units" that are generally seen at the grain boundaries were also found to occur in anti-phase boundaries.

5. The atomic density of the surface has a direct correlation with the magnitude of distortion created by the surface.

6. There is a greater probability that a vacancy will form near a grain boundary. The effect of the grain boundary on the vacancy in most obvious up to a distance of 5 Å away from the boundary.

7. The formation of an Aluminum vacancy is more favorable than a Nickel vacancy. However, the activation energy for migration of a Ni vacancy to the boundary is greater than that for an Aluminum vacancy.

8. Although the absolute values of energy obtained in this studied are not very close to the experimentally observed ones, the relative behavior of atoms compares well with the results obtained from other models.

9.0 Suggestions for Further Study

1. Displacement calculations based on the development in chapter two can yield accurate results for atoms that are relatively far from the defect. The Green's function technique can be used to calculate the displacements of atoms in Region II. Region II is generated during the relaxation procedure. Such a procedure would require the experimental determination of the Kansaki forces and matrix mathematics to obtain the Greens function matrix.

2. Experimental observations using advanced microscopy techniques such as the recently developed scanning tunneling microscopy could provide supportive evidence for the present simulated result that could bring about a radical change in the in the present understanding of lattice theory. Surface rippling and the behavior of atoms in the vicinity of the surface could be directly observed.

3. The FORTRAN program used in this study could be used to study various defect interactions. If the potentials for Boron can be estimated to a reasonable accuracy the activation energy gradient for migration of Boron to the boundary and the reason for its beneficial effects could be ascertained.

4. By creating a vacancy and an interstitial at the same time, the least distance of recombination and effect of atom type could be studied. By generating the vacancy at all possible non equivalent sites around a boundary, a vacancy formation contour and a path of least energy of a vacancy could be identified.

5. It is apparent from our results that given the activation energy Nickel vacancy has a higher probability of migrating to the boundary than an Aluminum vacancy. A test sample of Ni_3Al that has been thermally treated to provide the activation for migration could be used experimentally substantiate this result. If such a specimen is made to undergo a catastrophic, intergranular failure and tested for surface composition, the fractured surface should show more Aluminum than Nickel.

10.0 References

1. C. T. Liu et al, Acta Metall., **33** , 213, (1985).

2. K. Aoki, and Isumi, Nippon Kinsoku Gakkashi, **43** , 1190, (1979).

3. V. Paidar, Acta Metall. **33**, 1803, (1985).

4. M. J. Norgett, R. C. Perrin, and E. J. Savino, J. Phys. F 2, **L 73** , (1972).

5. Proc. of a Conf. on **"Properties of Atomic Defects in Metals"** , Argonne, Illinois, U. S. A. October, (1976), J. Nucl. Mater., (1978).

6. D. Frederick, and T. S. Chang, **"Continuum Mechanics"** , Allyn and Bacon, (1972).

7. Dr. S. Rao, Seminar on **"Lattice Defects"** , Virginia Tech, (1987).

8. A. A. Maradudin, E. W. Mantroll, G. H. Weiss and I. P. Ipatova, **"Theory of Lattice Dynamics in the Harmonic Approximation"** , 'Solid State Physics suppliment, V. 3', Academic Press. N. Y. (1971).

9. P. H. Dedrichs, J. Phys. F: Metal Phys., **3**, 471 (1973).

10. E. J. Savino and S. Rao, Private Communication.

11. P. A. Flin, and A. A. Maradudin, Ann. Phys., (N. Y.) **18** , 81 (1962).

12. V. K. Tewary, Adv. Phys., **22** , 757, (1973).

13. I. M. Torrens, "Inter atomic potentials", Academic press, (N. Y.), (1972).

14. J. M. Eridon, Dissertation, "Metastable Phase Formation in Ion Irradiated Nickel-Aluminium Alloys", University of Michigan, (1986).

15. P. Beauchamp, R. Taylor and V. Vitek, J. Phys. F: Metal Phys. **5** , 2017 (1975).

16. E. S. Machlin. Acta metall **22** , 95, (1974).

17. E. S. Machlin. Acta metall **22** , 109, (1974).

18. E. S. Machlin. Acta metall **22** , 1433, (1974).

19. K. Madea, V. Vitek and A. P. Sutton Acta metall. **30** , 2001 (1982).

20. M. S. Dan and M. I. Baskes, Phys. Rev. **B29** , 6443 (1984).

21. A. F. Vorter, to be phublished.

22. J. H. Rose, J. R. Smith, F. Guinea, and J. Ferrante, Phys. Rev. 1329, 2963, (1984).

23. S. P. Chen, A. F. Vorter, and D. J. Srolocitz, Scripta metall, **20** , 1389 (1986).

24. E. J. Savino, and D. Farkas, to be published in Phil. Mag..

25. A. P. Sutton, and V. Vitek, Phil.Trans. R. **A 309** , (1983).

26. D. Hull, "Introduction to dislocations", Pergamon Press, (1975).

27. J. P. Hirth and J. Lothe, " Theory of Dislocations" , Wiley Interscience, (1982).

28. A. P. Sutton, International Metals Reviews, **29** , 377 (1984).

29. V. Rangarajan, Thesis, "A Study of Grain boundary Structures in Boron doped Ni_3Al" , Virginia Tech, (1985).

30. L. S. Shivindlerman and Strammal Acta metall. **33** , 1735 (1985).

31. R. W. Ballufi, Met Trans., **13-A** , 2069, (1982).

32. D. Farkas, Scripta Metall. **19** , 467, (1985).

33. R. W. Ballufi, Conf. Proc. on "Grain Boundary structure and Kinetics" , at Wisconsin 297, (1979).

34. A. N. Aleshin et al Scripta Metall. **19** , 1135 (1985).

35. V. Vitek, Y. Milnonishi, and G. J. Wang, J. Phys., **46** C4-1971 (1985).

36. F. D. Tichelaar and F. W. Schapink, Phil. Mag. **A 54** , 2, L55 (1986).

37. P. M. Hazzledine and Sir P. Hirsch, M.R.S. symp. Proc. **81**, 75, (1986).

38. A. G. Croker et al Surf. Scnc. **34** , 97 (1984).

39. D. Farkas et al, Proc. of Conf. M. R. S. New Hampshire (1987).

40. S. P. Chen, A. F. Vorter and D. J. Scrolovitz, Phy. Rev. Letter. **57** , 11, 1308 (1986).

41. D. Farkas and Rangarajan, Acta. Metall, **35** , 353, (1987).

42. R. W. Ballufi and G. B. Olson, Metall. Trans. A **16** A 529, (1985).

The vita has been removed
from the scanned document